Virus-host metabolic interactions: using metabolomics to probe oxidative stress, inflammation and systemic immunity

Schoeman, J.C.

Chapter 2

Development and application of a UPLC-MS/MS metabolomics-based comprehensive systemic and tissue specific screening method for inflammatory-, oxidative- and nitrosative stress

Johannes C. Schoeman, Amy C. Harms, M. van Weeghel, Rob J. Vreeken, Ruud Berger, and Thomas Hankemeier.

Manuscript submitted for publication

Abstract

Oxidative stress and inflammation are underlying pathogenic mechanisms associated with the progression of several pathological conditions and immunological responses. Elucidating the role of signalling lipid classes, which includes amongst others the isoprostanes, nitro-fatty acids, prostanoids, lyso-sphingolipids, and lysophosphatidic acids, will create a snapshot into the cause and effect of inflammation and oxidative stress on the metabolic level. Here we describe a fast, sensitive, and targeted UHPLC-MS/MS metabolomics method enabling the qualitative measurement and biological elucidation of 17-isoprostanes as well as their respective isomeric prostanoid mediators, three nitro-fatty acids, four lysosphingolipid mediators, and 24 lysophosphatidic acid species from serum as well organ tissues including: liver, lung, heart, spleen, kidney and brain. Application of this methodology to paired mice serum and tissue samples revealed tissue and serum specific stress and inflammatory readouts. Little correlation was found between homeostatic localised (tissue) metabolite levels compared to the systemic (serum) circulation. The application of this methodology to future studies will enable us to explore the role of signalling lipids in the metabolic pathogenicity of stress and inflammation during health and disease.

Background

Oxidative stress is characterised as a condition where levels of reactive oxygen species (ROS) necessary for cellular redox biology [1–5] increases above the cellular antioxidant threshold leading to macromolecular damage [6], and is an underlying pathogenic mechanism associated with the progression of most pathological conditions [7–10]. More recent however, it has been argued by Schieber & Chandel that it is the exploited signalling capacity of hydrogen peroxide (H_2O_2) displaying hormesis, which underlies many physiological conditions, and that oxidative stress is a classification term for the cellular damage caused by uncontrollably high levels of ROS [11]. Hormesis can be defined as a biphasic dose response, with low concentrations resulting in beneficial effects and high concentrations resulting in inhibitory or toxic effects [12]. The need to understand the intricate (cause and effect) relationship between oxidative stress and inflammation has been gaining momentum in recent years, as elucidating these mechanisms may allow novel therapeutic approaches. Due to the cumbrousness and unreliability in measuring free radicals, downstream products that are reflective of a failed cellular anti-oxidant capacity leading to oxidative damage, present ideal metabolomics targets to evaluate oxidative stress. The biological membrane bound glycerophospholipids are reservoirs for unsaturated fatty acids, vulnerable to free radical attacks [13,14]. Non-enzymatic oxidation of these unsaturated fatty acids affects and impairs membrane integrity and function, leading to cellular stress. Isoprostanes are stable prostanoid-like lipid peroxidation markers, with their readout regarded as the golden standard to evaluate oxidative stress *in vitro* and *in vivo* [15,16]. Similarly, nitrosylated lipids (NO_2-FAs) synthesised via reactive nitrogen species (RNS) can be used to evaluate nitrosative stress within a system [17]. While the downstream readouts of oxidative and nitrosative stress are effective for indirectly measuring the dysregulation in the ROS and RNS levels, measurement of lipid signalling metabolites implicated as causative of inflammation are also of importance. During innate immune activation via pathogen recognition receptors, the generation of ROS via the mitochondria and NADPH oxidases, and its downstream signalling, are essential for the activation of inflammatory pathways [18,19].

Several lipid classes including the prostaglandins, lysosphingolipids (LSLs) and lysophosphatidic acids (LPAs) have been implicated in the activation of signalling pathways regulating inflammation, oxidative stress and cell proliferation among other physiological responses via dedicated cellular receptors. Prostaglandins are enzymatic lipid signalling mediators, playing an active role in inflammation, pain and immunomodulation, conducting their signalling through dedicated prostaglandin specific G-coupled cellular receptors [20,21]. Prostaglandins are enzymatically synthesised (*de novo*) via the cyclooxygenase mediated oxidation of essential fatty acids. They are also structural isomers of the above mentioned isoprostanes. The LSL include the metabolites sphingosine (Sph) and sphingosine-1-phosphate (S1P). The various roles of S1P in innate and adaptive immunity include among others immune cell trafficking, differentiation, immune-surveillance [22–24] and it has also been implicated in inflammatory and oxidative stress signalling [25]. Lysophosphatidic acids are the simplest phospholipid species, an essential intermediate in de novo glycerophospholipids and triglyceride synthesis. Apart from their metabolic roles, LPAs and cyclic-LPAs are also active signalling mediators which are able to influence cell proliferation, immunological functions and inflammatory signalling through five dedicated G-protein-coupled cellular receptors [26,27]. Development of a targeted metabolomics method for the measurements of isoprostanes, nitro-fatty acids, prostaglandins, LSL, and LPAs as well as the cyclic-LPA species presents an opportunity to study the cause and effect of oxidative stress, inflammation and cell proliferation at

the metabolic level. Secondly, studying the combined effect of these signalling mediators will be particularly helpful as these signalling molecules could have distinct and sometimes even opposing functions.

Currently some of the biggest challenges facing targeted metabolomics are: i. adequate sensitivity, for the detection of low endogenous concentrations, ii. optimal chromatographic resolution, to separate structural isomers for accurate measurements and class assignment, iii. high throughput screening, as well as iv. appropriate experimental study design [28,29]. The study design is essential to adequately answer biological questions. The choice of experimental group and inclusion criteria together with the choice of sample material will determine the usability and suitability of metabolomics to address biological questions. Bio-fluids as sample material including serum, plasma and urine provide a more systemic metabolic readout, whereas tissue samples mainly reflect a localised metabolic readout. Although the importance of metabolites and especially signalling lipid mediators is obvious, many questions still remain about their function, in part because only a few tools are able to accurately measure them location specific *in vivo*. Adequate addressing the above critical points during a metabolomics study results in a powerful methodology for biomarker discovery, elucidating pathogenic mechanisms, predicting disease severity, risk stratification and measuring therapeutic intervention.

Here we describe a fast, sensitive, and targeted UHPLC-MS/MS metabolomics method enabling the measurement of 17-isoprostanes as well as 11 isomeric prostaglandin mediators, three nitro-fatty acids, four LSL mediators, and 24 LPA species. Application of the developed methodology to patient derived serum and tissue samples will help in determining the underlying links of inflammation and oxidative stress in disease. We applied the developed methodology to a homeostatic mouse model with paired tissue and serum samples, providing a stress and inflammation readout for serum as well as brain, lung, liver, heart, kidney and spleen tissues.

Methods

Chemicals and reagents

Ultra-performance liquid chromatography (UPLC)-grade acetonitrile, isopropanol, methanol, ethyl acetate, and water were purchased from Biosolve B.V. (Valkenswaard, the Netherlands). n-Butanol was obtained from Boom B.V (Meppel, the Netherlands). Acetic acid, ammonium hydroxide, butylated hydroxy-toluene (BHT), ethylenediaminetetraacetic acid (EDTA) and ammonium acetate were from Sigma-Aldrich (Zwijndrecht, the Netherlands). Sodium dihydrogen phosphate dehydrate and citric acid were obtained from Merck (Darmstadt, Germany). Standards and deuterated standards were purchased from Cayman Chemicals (Ann Arbor, MI, USA) and Avanti Polar Lipids (Alabaster, AL, USA).

Internal standards and standard curve preparations

Standard and deuterated standard stock solutions were prepared in methanol containing BHT (0.2 mg/mL). A calibration stock solution was made, with a concentration of 1304 nM (labelled C8) and this solution was diluted to levels C7 through C1, which is the lowest calibration level at 0.75 nM. Supplementary Table S2.1

provides a schematic overview of the stock solution concentrations as well as spiked calibration concentrations used during this study and method validation procedures.

Biological samples

Human serum

Control human serum used in the method validation was purchased from Harlan Sera-Lab, Leicester, United Kingdom (tested negative for HIV antibody and hepatitis B surface antigen).

C57BL/6 mice sample collection

C57BL/6 mice were housed at 21 ± 1 °C, 40-50% humidity, on a 12-h light-dark cycle, with ad libitum access to water and a standard rodent diet. Mice were anesthetized in isoflurane and euthanized by cervical dislocation. After opening up the chest cavity, blood was collected using a 22-gauge needle from the heart and left to coagulate on ice. The heart, lungs, liver, spleen, kidneys and brain were harvested in that sequence, cleaned of excess visceral fat, hair, tissues and blood, and snap frozen in liquid nitrogen. After the blood has coagulated on ice for ~30 minutes the samples were centrifuged at 2000 x g at 4°C for 10 minutes, where the serum was transferred to a clean Eppendorf vial, snap frozen and stored at – 80 °C. All procedures were approved by the institutional review board for animal experiments at the Leiden University Medical Center (Leiden, The Netherlands).

Extraction procedures

Serum extraction

150 µL serum aliquots were thawed on ice after which 5 µL antioxidant (0.2mg BHT and 0.2 mg EDTA) solution and 10 µL of ISTD solution were added and the serum was briefly vortexed. Samples were then acidified through the addition of 350 uL of 0.2 M citric acid and 0.1 M disodium hydrogen phosphate buffer at pH 4.5. Liquid-liquid extraction (LLE) was accomplished with the addition of 1 mL of a 1-butanol: ethyl acetate (BuOH: EtOAc) (1:1 v:v) solution. Samples were mixed for 2 min, centrifuged for 10 min at 4°C and 16 000 rcf after which 900 µL of the upper organic phase was collected and transferred to a clean 2 mL tube. The LLE extraction was repeated a second time by adding 400 µL BuOH saturated with water and 400 µL EtOAc to the remaining aqueous phase. After mixing and centrifugation, 800 µL of the organic phase was collected and the total organic fraction was dried under vacuum. 40 µL of ice cold 90 % MeOH injection solution was added to the dried residue as reconstitution solution. Reconstituted samples were vortexed prior to centrifugation for 10 min at 4°C and 15 700 rcf and subsequently transferred to inserts in injection vials prior to LCMS analyses and stored in the autosampler at 5 °C.

Tissue extraction

Snap frozen tissue samples were transferred to the freeze dryer, where tissues were dried overnight, mechanically homogenised, aliquoted and stored at – 80 °C prior to extraction. Dried tissue aliquots of 5 mg

were suspended in 200 µL of a 0.2 M citric acid and 0.1 M disodium hydrogen phosphate buffer at pH 4.5 to which approximately 500 mg of 0.5 mm stainless steel beads (Next Advance, Averill Park, NY, USA) were added. 5 µL antioxidant (0.2mg BHT/EDTA) and 10 µL of ISTDs solution were added and tissue samples were homogenised in the bullet blender at maximum speed for 10 minutes. Afterwards samples were centrifuged for 30 seconds at 4000 rcf followed by the addition of another 150 µL pH 4.5 buffer as well as 1 mL of a BuOH:EtOAc (1:1 v:v) solution. The collection of the organic phase and repeated extraction steps follows as detailed above for the serum extraction.

Targeted LC-MS/MS analyses

Low pH runs

Liquid chromatography was performed using a Shimadzu LCMS-8050 (Shimadzu, Japan) and an Acquity BEH C18 column (50 x 2.1 mm, 1.7 µm) (Waters, Milford, MA, USA) maintained at 40 °C. The mobile phases consisted of (A) H2O + 0.1 % Acetic Acid, (B) ACN: MeOH (7.5:2.5, v:v) + 0.1 % Acetic acid, and (C) IPA with a flow rate of 0.7 mL/min. To increase the column load-ability a stacked injection was used which consisted of plugging 10 µL sample volume with 20 µL of mobile phase A before injecting this "solution stack" onto the column, with the 20 µl first entering the column. The analytes eluted using a gradient starting at 5 % B, 0% C to 75 % B, and 25 % C between 0 and 9 min; the final conditions were held for 1 min after which the column is re-equilibrated to starting conditions from 10.15 to 13 min.

High pH runs

Liquid chromatography was performed using the Shimadzu LCMS-8050 (Shimadzu, Japan) and a Kromasil EternityXT-1.8 C18 column (50 x 2.1 mm, 1.8 µm) (AkzoNobel, the Netherlands) maintained at 40 °C. The mobile phases consisted of (A) H2O + 5 mM Ammonium acetate + 0.0625 % ammonium hydroxide and (B) ACN: IPA (8:2, v:v) + 0.1 % ammonium hydroxide with a flow rate of 0.6 mL/min. The injection volume was 5 µL. The metabolites were eluted using a linear gradient starting at 10 % B to 100 % B in 5 min, the conditions were kept at 100 % B for 0.75 min after which the column was re-equilibrated to starting conditions from 5.75 to 8 min.

MS/MS analyses

The Shimadzu LCMS-8050 consists of a UHPLC system connected to a triple quadrupole mass spectrometer with an ESI source. The ESI source parameters were as follows: Interface temperature 300 °C, desolvation lines (DL) temperature 250 °C, heat block temperature 400 °C, with the nebulizing gas flow at 3 L/min, heating gas flow at 10 L/min, and the drying gas flow at 10 L/min. The analytes and ISTDs were measured using MRMs in either positive or negative ion mode with a complete optimised target list (Collision energy and dwell time) in Table S2.2. During the development procedure, the most specific or sensitive transition was selected to avoid interferences and increase detection limits.

The target list (Table S2.2) included both metabolites identified through the use of commercially available standards, as well as putatively identified metabolites. The Putatively identified metabolites were

identified using different MS modes and expected transitions, explained in more detail in the Supplementary Methods.

Method validation criteria

Method performance was investigated and included linearity, limits of detection (LOD), retention time stability, inter and intra-day precision, extraction recovery, matrix effect, and ion suppression.

LOD and linear range

Calibrations curves were prepared in four replicates with 7 concentrations ranging over 4 orders of magnitude to assess the LOD (using blank matrix) and linear range (using control serum). For each calibration curve, the ratio of the analyte area and its corresponding IS area was plotted against its nominal concentration with no weighting factor being applied. LOD was determined as the lowest concentration that resulted in a peak with a signal-to-noise ratio (S/N) > 3 using the ASTM method.

Retention time stability

Retention time stability reflects the stability of the chromatography over progressive runs, to ensure correct peak identification based on retention time during data processing. The retention time stability was investigated through determining the RSD values of the metabolites retention time across a sequence of 100 injections. Retention times are considered stabile if the RSD < 1%.

Intra and Inter day precision

Precision is defined as the closeness of the measurements of individual samples, when the procedure is applied to multiple aliquots of a homogenous matrix, hence precision is reported as the relative standard deviation (RSD) of the measurements [30]. The method is considered to be precise if the RSD is below 15% for mid calibration range metabolites, or 30% for the lower limit of detection range metabolites. Intra-day precision was determined by calculating the RSD of four replicate measurements of control serum at three different levels (low, medium, high). Inter-day precision was assessed by comparing the closeness of the quadruplicate samples at each level over three days.

Analytical recovery

Recovery reflects the extraction efficiency of the LLE procedure for the metabolites in a specific biological matrix and should be reproducible (low RSD). Both the serum and different tissue recoveries were determined by comparing the response of an ISTD spiked in sample before LLE to the response obtained from the ISTD spiked after LLE. Serum recoveries were determined in quadruplicate using control serum aliquots at three different levels (low, medium, high; Table S2.1). Tissue recoveries were determined in quadruplicate using control tissue aliquots at one level (medium; Table S2.1).

Matrix effect and ion suppression.

The matrix effect can be explained as the interference of matrix compounds during sample preparation and interferences in ionization efficiency resulting from co-eluting compounds present in the biological matrix, and must be evaluated. If a matrix effect is affecting the analyte signal, it does not necessarily imply that the method is not valid, but in this case the added ISTD must be able to correct for the matrix effects. The matrix effect was assessed by spiking the non-endogenous ISTD to the matrix and to an academic blank solution, and by comparing the ISTD responses (i.e. peak areas without further corrections) obtained from the spiked blank and the ISTD responded obtained from the biological matrix spiked with ISTD before LLE extraction. Ion suppression only, i.e. without the effect of sample preparation, was also assessed using the ISTDs, through comparing the ISTD responses obtained from blank and biological matrix spiked with ISTD after LLE extraction. For serum, matrix effect and ion suppression were determined in quadruplicate from control serum and blank matrix aliquots at three different spiked ISTD levels (low, medium and high; Table S1). For tissues, matrix effect and ion suppression were determined in quadruplicate from control tissues and blank matrix aliquots at a single spiked ISTD level (medium; Table S2.1).

Data processing and statistical methods

Peak detection, integration and quantification were done using the Shimadzu LabSolution software package V5.65. Relative ratios of metabolite peak areas to their corresponding internal standards were used for statistical analyses. Principal component analyses (PCA) and heatmaps based on Euclidean distance measure and Ward clustering Algorithm were performed using the R script–based online tool Metaboanalyst v3.0, a comprehensive tool suitable for analysing metabolomics data [31]. Spearman correlation coefficients were calculated using SPSS version 23.0 (IBM Corp., Armonk, NY). During the intergroup correlation analyses, each metabolite was correlated against itself, thus no multiple testing correction was performed. Significant correlations were defined as a Spearman's coefficient: $r < -0.7$, $r > 0.7$ and p-values < 0.05.

Results & Discussion

Method development

The development of a high throughput method for the quantification of a panel of inflammatory, oxidative and nitrosative stress markers in serum (systemic readout) and tissues (localised readout) faced five main challenges. Firstly, the dynamic range of endogenous concentrations, ranging from low nano molar (nM) for the isoprostanes, prostaglandins and NO_2-FAs [32,33] to medium to high nM ranges for the LPAs and LSLs [34,35], demanded optimization of every step to guarantee the optimal limits of quantification. Due to the diverse chemical nature of these metabolites, LLE was chosen as the sample-prep method of choice. The pH 4.5 buffer was used to ensure stability and a negative charge of the target metabolites. In the presence of strong acids the obtained values of LPAs in an analysis can be artificially increased ex-vivo by either enzymatically or chemically hydrolysis of lysophosphatidyl cholines (LPCs) and ethanolamines (LPEs) to form LPA [35,36]. The composition of 1-butanol and ethyl acetate used during LLE ensured excellent recoveries of our target lysophospholipids (LPAs and LSLs) [35,37] as well as oxidised and nitrated lipids. The polar nature of the organic solvents used during

LLE also reduced background noise and matrix interferences by preventing the extraction of non-polar and neutral lipids.

Secondly, optimised, MS compatible, chromatography is necessary for adequate metabolite separation which can distinguish between the structural isomers of isoprostanes and prostaglandins (Supplementary Figure S2.1). Furthermore, separation between different lysophospholipid classes is also necessary for accurate measurements of LPA levels, as insource fragmentation of more complex lysophospholipids (LPS - serine, LPI - inositol, LPG – glycerol, LPC - choline, LPE - ethanolamine) can result in increased LPA levels in the case of chromatographic co-elution (Figure S2.2). Optimising the chromatographic run proved the most challenging aspect and required compromises in i. mobile phase conditions including organic solvents, salt concentrations, pH modifiers ii., gradients and run time as well as iii. different C18 stationary phases; no single chromatographic run was found to be suitable for the analysis of the selected panel of compounds. Table S2.3 provides an overview of the conditions tested and each class's response in the selected setup. In order to be able to analyse all compound classes, the chromatography was split into two runs namely i. a low pH run analysing the isoprostanes, prostaglandins, NO_2-FA as well as sphingosine and sphinganine (Spha) (Figure 2.1 A) and ii. a high pH run analysing the LPA classes as well as S1P and Spha1P (Figure 2.1 B).

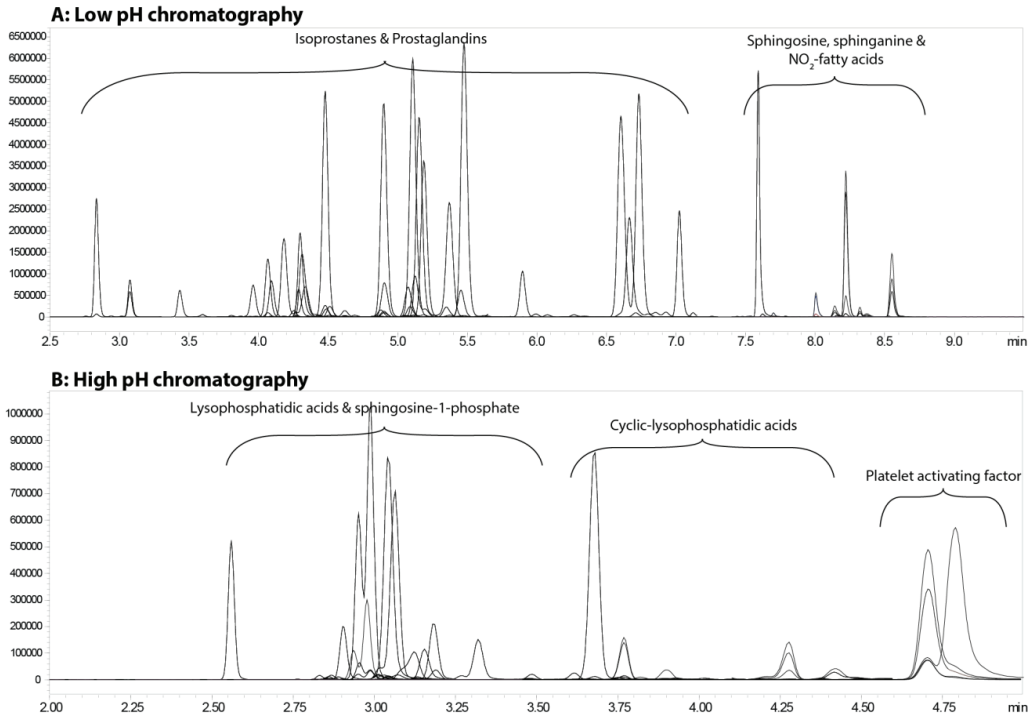

Figure 2.1: LC-MS/MS showing A – the low pH run and B – the high pH run.

Thirdly, optimization of the mass spectrometric detection is necessary to ensure accurate quantification of the endogenous metabolites over a large dynamic range. A tandem mass spectrometry approach using dynamic multiple reaction monitoring was chosen for enhanced sensitivity. MS parameters were individually optimised for each compound using commercially available standards. The MS optimised compounds and their respective deuterated ISTDs were evaluated for MRM cross-talk and no interferences were observed. Possible cross-talk between MRMs was further reduced by using a 2 msec pause time between each MRM transition so that ions of the previous transition were not interfering. The fast polarity switching of 5 msec of the LCMS-8050 and optimised chromatography ensured no drop in sensitivity when measuring in both the negative and positive MS modes during chromatographic runs.

Fourthly, ISTDs are necessary to compensate for: i. variation in extraction efficiency during LLE, ii. instrument variability, and iii. ionization efficiency. When possible, deuterium labelled standards, usually containing 4 to 11 deuterium atoms, were used as ISTD to ensure MRM discrimination from the endogenous metabolites. These labelled ISTDs have very similar properties in terms of extraction, recovery and elution compared to the endogenous unlabelled metabolite. Due to the limited availability of deuterated LPA's and LSL's, uneven chain fatty acid (C17:0) species were used as ISTDs for the quantification of LPAs and LSLs. When no direct/deuterated ISTD was available for a metabolite, the closest eluting ISTD to that endogenous metabolite of the same class was selected as ISTD.

Lastly, measuring a localised response requires the use of tissue as biological matrix. As different tissues have vastly different functions, it is presumed that each tissue will have a unique homeostatic profile of stress and inflammatory mediators. Tissue sampling also presented some matrix specific challenges, and the choice between using wet or dry material is not always clear and could influence extraction repeatability and efficiency. In this study we used freeze-dried tissues, which were mechanically homogenised leading to more reproducible sample aliquots. Tissue samples were subsequently further homogenised during the LLE extraction in the extraction buffer, using 0.5 mm stainless steel beads and a bullet blender.

Method validation

The targeted metabolomics profiling platform was validated to assure its robustness and reproducibility in providing quality data for biological interpretation. As the selected target metabolites are mostly present in biological matrices including serum and tissues, no "blank" matrix was available and different validation matrices had to be used for different experiments [38,39]. Thus for calibration lines investigating detector linearity, a blank matrix of pure water was selected. For investigating intra- and inter-day precision, homogenous biological matrix aliquots (commercially available serum) as well as blank matrix (water) were spiked with the panel of compounds. Recoveries and matrix effects were studied using only exogenous ISTDs spiked in homogenous biological matrix aliquots.

Serum validation

Investigating the linearity and sensitivity of our metabolomics platform using the LCMS-8050 provided satisfactory results. Overall, the 40 standards representative of the different endogenous compound classes in

the targeted metabolomics platform showed a good linear response with 87.5 % of the metabolites having an R^2 >0.99 while the remaining 12.5 % ranged between 0.96 < R^2 <0.99 (Table 2.1). Regarding sensitivity, LOD was determined as the lowest amount of standard necessary to provide an S/N >3 while still being within the linear range of the calibration curve (Table 2.1), and were well below reference physiological levels for most relevant compounds. The prostaglandins and isoprostanes had LODs of around 0.09 nM corresponding to an LOD in serum between 20 - 40 pg/mL for the different metabolites. The LOD's of LPAs and LSLs were higher compared to the other classes due to increased background noise, but were still well below physiological levels.

Retention time stability was investigated for both the low pH run compounds as well as the high pH run compounds across 3 different batches measured on 3 separate days. Retention time stability is critical to ensure correct peak identification over different sample batches, as a number of structural isomers of the prostaglandins and isoprostanes have to be differentiated, and co-eluting lysophospholipids can influence the response of LPA's due to insource fragmentation. The low pH chromatography preformed best with the highest RSD or the retention time being 0.55% for 8-iso-15-keto-PGE_2 (Table 2.1). The high pH chromatography had slightly higher RSDs for retention times, with LPA C18:0 showing an RSD of 2.25% (Table 2.1). The 2.25% RSD corresponds to a standard deviation of 0.075 mins or 4.5 seconds which still allows correct peak identification, although care should be applied during peak picking across batches.

Investigating the intra-day precision was found to be good across the three investigated levels in a serum matrix, with 100% of metabolites having an RSD < 15% at C4, and 73% an RSD < 15% at the C2 level (Table 2.1). Next we assessed the overall reproducibility considering variables such as extraction, measurement days and instrument related issues, including injection variation or MS drift. Inter-day precision gave equally satisfying results with 77% of metabolites having an RSD < 15% and 94% an RSD < 30% across the three investigated levels (Table 2.1). Overall the LPAs and LSL had higher RSDs, which presumably can be due the lack of deuterated ISTDs as then uneven (C17:0) acyl derivatives of these metabolites were used. Recovery experiments demonstrated minimal loss of metabolites during the LLE serum extraction procedure. Averaged ISTD recoveries over three consecutive days were close to 100% (Figure 2.2 A, Table S2.4). Higher extraction variation was observed in the LPAs, LSLs and NO_2-fatty acids compared to the isoprostanes and prostaglandin ISTDs, the highest RSDs were still well below 15% which also provides a further glimpse into the precision of the method. The ion suppression and matrix effect values (Figure 2.2 B, Table S2.4) were close to 1 for most of the metabolites, an indication that the extraction method and the serum matrix have minimal impact during MS/MS detection for most of the targeted metabolites. Some of the LSL and LPA internal standards did showed some ion enhancement, and a few compounds showed some ion suppression, especially the NO_2-fatty acids.

Table 2.1: Methodology validation characteristics in serum.

Compound name	Linearity (R2)	LOD (nM)	RT stability (n = 3) * (% RSD)	Precision in serum (% RSD)					
				Intra-day			Inter-day		
				C2 - low	C4 - medium	C7 - high	C2 - low	C4 - medium	C7 - high
Lysophosphatidic acid									
aLPA C18:1	0.9709	12	0.79	19.9	8.8	27.3	11.5	8.5	30.1
cLPA C18:1	0.9856	1.2	1.41	10.7	11.2	16.4	26.0	12.9	12.5
LPA C20:4	0.9863	12	1.81	7.9	13.3	33.9	26.8	17.9	23.9
LPA C16:0	0.9752	1.2	1.88	2.9	14.4	7.7	26.2	11.6	25.3
LPA C18:0	0.9931	1.2	2.25	26.7	12.2	44.7	26.8	12.9	34.6
Lysosphingolipids									
Sph C18:1	0.9993	1.2	0.13	0.3	4.8	4.9	7.5	8.2	11
Spha C18:0	0.9951	1.2	0.28	21	3.3	18.8	13.6	9.8	16.7
S1P C18:1	0.9795	12	1.52	4.9	9.3	24.0	8.4	16.2	21.0
Nitro Fatty acids									
NO2-OA	0.9995	0.09	0.04	9.9	5.7	9.1	9.2	6.0	10.4
NO2-LA	0.9993	0.09	0.04	16.3	8.5	9.5	14.9	17.5	20.7
Prostaglandins									
2_3-dinor-11b-PGF2α	0.9998	0.09	0.21	20.8	8.3	9.8	13.8	6.6	5.5
PGE3	0.9989	0.09	0.26	12.2	1.6	18.9	7.0	9.2	12.6
PGD3	0.9996	0.09	0.21	7.2	8.8	15.2	7.7	6.6	7.7
PGF3α	0.9998	0.3	0.17	17.2	5.4	4.9	17.0	6.6	7.1
PGE2	0.9999	0.09	0.13	6.3	2.0	9.6	11.6	11.2	11.1
PGE1	0.9996	0.3	0.10	1.5	3.4	6.9	5.6	5.0	3.9
PGD2	0.9991	0.09	0.20	1.1	2.6	1.5	1.2	2.3	1.6
PGF1α	0.9995	0.09	0.09	29.8	13.1	18.8	89.0	15.3	12.2
PGF2α	0.9987	0.09	0.09	15.3	6.6	6.2	8.8	5.1	5.2
13_14-dihydro-PGF2α	0.9995	0.09	0.20	2.6	4.7	5.2	2.9	3.4	3.7
PGA2	0.9994	0.09	0.10	7.6	0.6	6.1	6.0	4.0	4.7
PGA1	0.9995	0.09	0.07	1.9	0.7	5.8	2.7	7.1	5.5
Isoprostanes									
2_3-dinor-8-iso-PGF2α	0.9995	0.09	0.25	9.5	2.7	3.6	11.4	4.3	3.9
8-iso-PGF3α	0.9995	0.3	0.16	3.5	2.1	2.8	150.0	4.5	8.0
8-iso-15-keto-PGF2β	0.9982	0.09	0.20	9.1	5.3	9.2	12.2	5.8	7.5
8-iso-15-keto-PGE2	0.9997	1.2	0.55	38.3	2.7	6.9	24.9	2.7	3.6
8-iso-15-keto-PGF2α	0.9976	0.09	0.13	2.6	4.0	2.3	15.9	8.1	11.6
iPF2α	0.9988	0.09	0.12	8.5	4.2	6.8	5.5	2.7	4.2
8-iso-15(R)-PGF2α	0.9991	0.09	0.12	10.4	10.2	9.7	16.3	12.1	13.8
8-iso-PGF1α	0.9989	0.09	0.23	1.1	4.0	3.9	3.7	4.1	3.2
8-iso-13_14-dihydro-PGF2α	0.9994	0.3	0.11	10.6	3.7	6.4	150.8	8.8	11.6
8-iso-PGF2α	0.9993	0.09	0.11	8.1	5.1	5.3	9.3	5.1	6.2
8-iso-PGE2	0.9997	0.09	0.12	5.9	4.2	2.2	10.9	19.2	1.7
8-iso-PGE1	0.9995	0.09	0.15	8.2	3.8	4.8	43.6	6.9	3.9
+- 5iPF2α	0.9998	0.09	0.10	5.8	2.5	5.2	6.2	5.9	7.2
8-iso-PGA2	0.9994	0.09	0.11	4.9	1.5	5.8	5.9	4.1	4.8
8-iso-PGA1	0.9993	0.09	0.42	27.4	9.3	5.7	21.7	7.6	5.9
8_12-iPF2α IV	0.9974	0.09	0.08	7.0	4.6	9.9	4.1	5.2	16.0

* Retention time (RT) stability was calculated over 3 separate batches on 3 separate days.

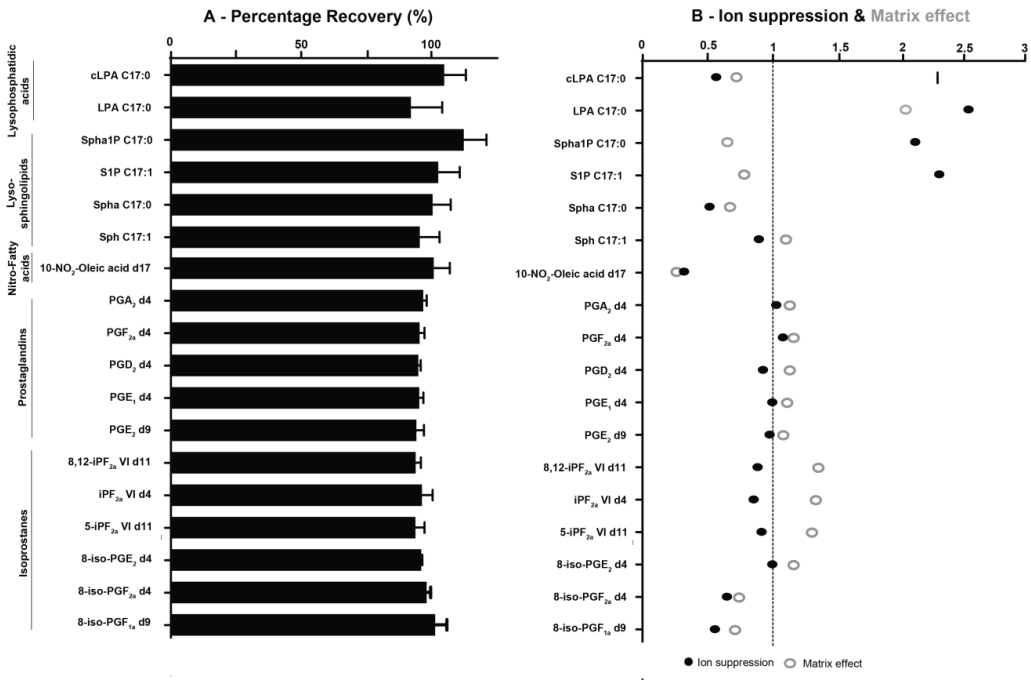

Figure 2.2: Methodology validation characteristics in serum. The ISTDs were investigated for A - recovery as well as B – Ion suppression and matrix effect, with 1 equal to no ion suppression or matrix effect. Error bars represent the RSD levels with n = 4.

Tissue application and performance characteristics

When addressing questions related to health and disease, serum provides a systemic readout for stress and inflammation markers. Measuring these metabolites in tissues on the other hand would provide a localised readout reflective of tissue homeostasis. Therefore, we also optimised the developed methodology for the extraction of heart, liver, lung, brain, spleen and kidney tissues and investigated the performance in each of these matrices. The performance characteristics evaluated for tissue samples included metabolite recoveries, matrix effects and intra-day precision. We attempted to compensate for tissue heterogeneity (biological variation) by using pooled dried tissues. These pooled samples were tissue specific and consisted of mechanically homogenised dried tissues, which were subsequently aliquoted to represent replicates of "homogenous biological tissues". These "homogenous biological tissue" replicates were then used to investigate intra-day precision, and with the addition of spiked ISTD we were able to assess the recovery and matrix effect for each tissue independently.

Comparing the different recoveries of the ISTDs from the six tissues reflected the diverse nature of these tissues (Figure 2.3 A, Table S2.5). It is important to note that the recoveries reported here do not assess the extent of metabolite recovery from tissue (solid to liquid) but only the eventual loss of targeted metabolites during the LLE sample prep. Overall the brain had the lowest levels of recoveries across the whole panel of ISTDs. We attribute this finding to the composition of brain tissue, consisting predominantly of very long chain lipid species. The polar nature of the organic solvent prevented the extraction of non-polar lipid species, therefore during the LLE a white lipid interphase was formed between the buffer and organic solvent and which probably negatively impacted the extraction efficiency of the panel of lipid signalling mediators. On the other hand, the kidney tissue had the highest metabolite recovery rates. The NO_2-FAs ISTD was poorly extracted with recoveries ranging from 36 to 55% across all tissues. Blank matrix (H_2O) samples following the same tissue extraction procedure, showed an extraction efficiency of around 80%. Investigating the reproducibility (n = 4) of 10-NO_2-OA-d17, revealed RSDs ranging from 4% in the spleen to 30 % in the lung. Hence although the NO_2-FAs has poor extraction efficiencies, in some tissues they can be reproducibly measured. In addition, these results suggest interactions of NO_2-FAs with tissue or protein during extraction, negatively impacting on the extraction efficacy of the NO_2-FAs. The isoprostanes and prostaglandins (except for PGA2-d4) had reasonable extraction efficiencies (70% - 100%) as did the LPA and LSL metabolites.

When investigating the matrix effect for different tissues, (Figure 2.3 B, Table S2.5) the brain tissue, having the lowest recoveries, also experienced the highest levels of matrix effect. The kidney, with its high recoveries, together with the spleen, experienced the least matrix effects for the majority of the compounds. Compounds eluting later in the LC-MS chromatogram experienced notably higher levels of ion suppression (and therefore higher matrix effect) compared to the early eluting isoprostanes and prostaglandins. This could be attributed to the co-elution of other lipid species, most possibly other lysophospholipid metabolites present in high concentration in the tissues and extracted during the LLE step; and these lipid species might be higher in brain, lung and liver compared to heart, kidney and spleen. Notably, NO_2-FAs experienced high levels of ion suppression during the LC-MS chromatographic run, and together with the reduced extraction efficiency of this class of metabolites highlight the challenges in measuring them. The use of ISTDs for the analysis of especially those metabolites showing higher ion suppression and matrix effects is therefore critical; these non-endogenous ISTDs should be spiked at the same concentration level for the same metabolite in different tissues and allow a better comparison across different tissues in biological studies, and this is true for semi-quantitative (as we did) as well as quantitative metabolomics measurements.

The intraday precision was determined for all commercially available endogenous metabolites spiked to the different pooled tissue samples (n=4) at the C4 (medium) level (Figure S2.3, Table S2.6). The intraday precision results showed the extraction method to be reproducible, with all six tissues showing around 90 % of detected metabolites having an RSD of lower than 30 %. For extraction of comparable metabolites from muscle tissue Alves et al. reported higher RSD values, but still found that individual sample (biological) variation was larger than replicate (procedure) variation [40]. It should be noted that the precision was especially good for those metabolites for which deuterated ISTD were available: both NO_2-OA and PGA_2 presented with RSD levels below 16% and 8% respectively across all six tissues (Table S2.6). Furthermore, comparing from serum to tissue,

we are able to generate a tissue specific stress and inflammatory readout in the tissue samples contributing to fully understanding the localised responses of these metabolites in health and disease.

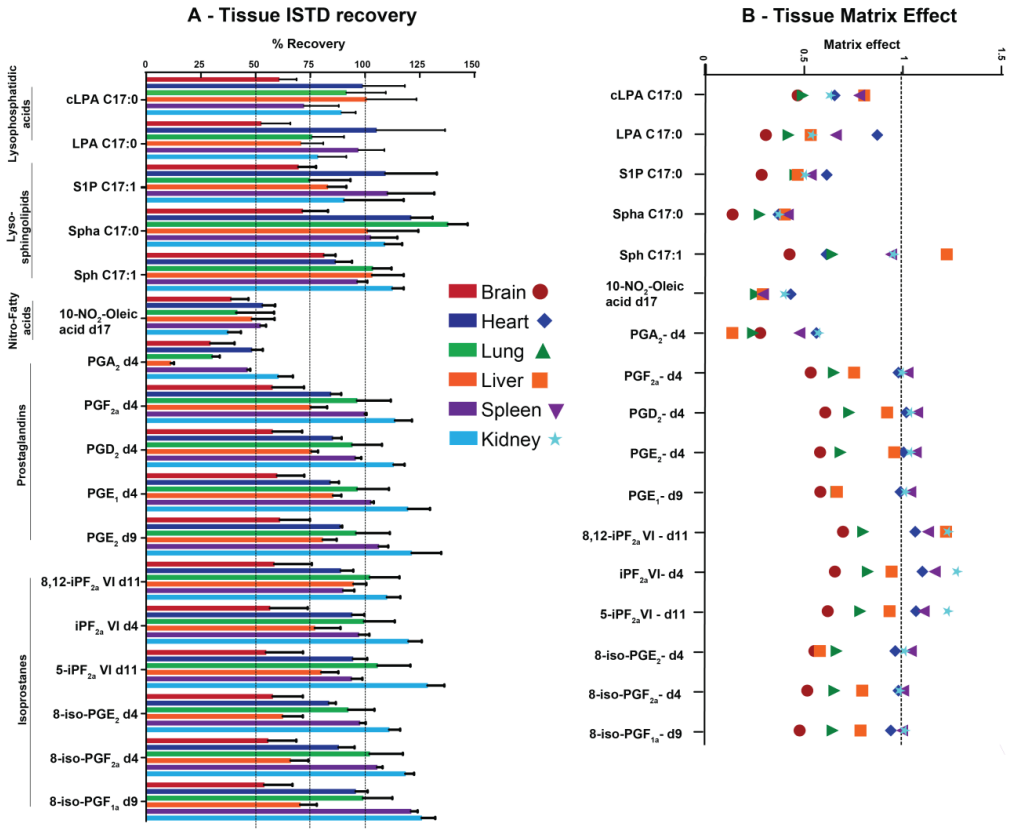

Figure 2.3: Methodology characteristics in six different tissues. The ISTDs were investigated for A - recovery (Error bars represent the RSD levels in n = 4) as well as B –matrix effect in brain, heart, liver, kidney, lung and spleen tissue samples.

Metabolic profiling of healthy paired mice serum and tissue samples

Applying the developed methodology to the paired tissue and serum samples of eight healthy C57BL/6 mice, we were able to create a homeostatic stress (oxidative and nitrosative) and inflammatory metabolic profile. Of the seven biological matrices investigated, the spleen had the highest number of metabolites (53 of 60 metabolites) detected with serum having the lowest number (35 of 60 metabolites). This result can be expected as most of these metabolites are signalling mediators which are produced locally. We also compared the variation of each metabolite due to the analytical variation (QC samples) to the biological variation of that metabolite (in different biological samples) on the endogenous metabolite levels in the different tissues (Table S2.7). For a simplified overview in Table S2.7, we averaged the RSDs of the metabolites detected within a class in the

different tissues. In almost all cases the procedural RSDs were significantly lower compared to the biological variation, comparable to the findings for other metabolites reported by Alves et al. [40].

Next, we investigated the natural projection of the metabolite levels in the various tissues and serum samples using unsupervised multivariate PCA. Inspection of the PCA results revealed that the samples of different tissue types and serum were completely separated as shown in Figure 2.4. The serum samples had the highest biological within sample-type group variation, while the tissues groups clustered more closely together. The large variation present between the different serum samples emphasises its function as a circulatory system within the body, connecting the different tissues and organs leading to a unique readout characteristic for the study subject. The different number of metabolites detected within the different tissues contributed to the complete PCA separation. Subsequently, we compiled a data set consisting of only the six tissues and only metabolites found in all tissues, and redid the PCA analyses (Figure S2.4). Even after reducing the data set, still clear differentiation between the six tissues was still observed, emphasising the tissue specific stress and inflammatory profile, and not due to metabolites only detected in one or a few but not all tissues.

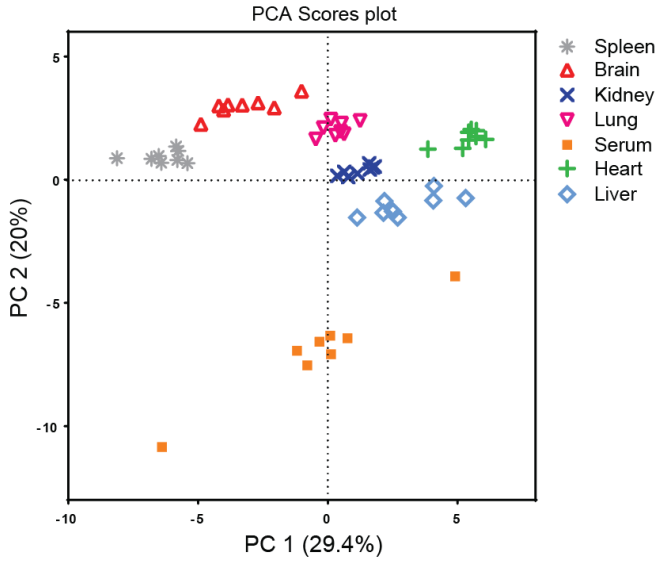

Figure 2.4: PCA of the paired tissue and serum samples of 8 healthy C57BL/6 mice. Complete differentiation is seen between the 6 different tissues types and serum.

To compare the different metabolite levels in the different tissue samples, heatmaps were used to visualise the individual measurements. The signalling lipid profile was split into the prostaglandins (Figure 2.5 A), the isoprostanes and NO_2-FAs (Figure 2.5 B) and the lysophosphatidic acids and lysophingolipids (Figure 2.5 C).

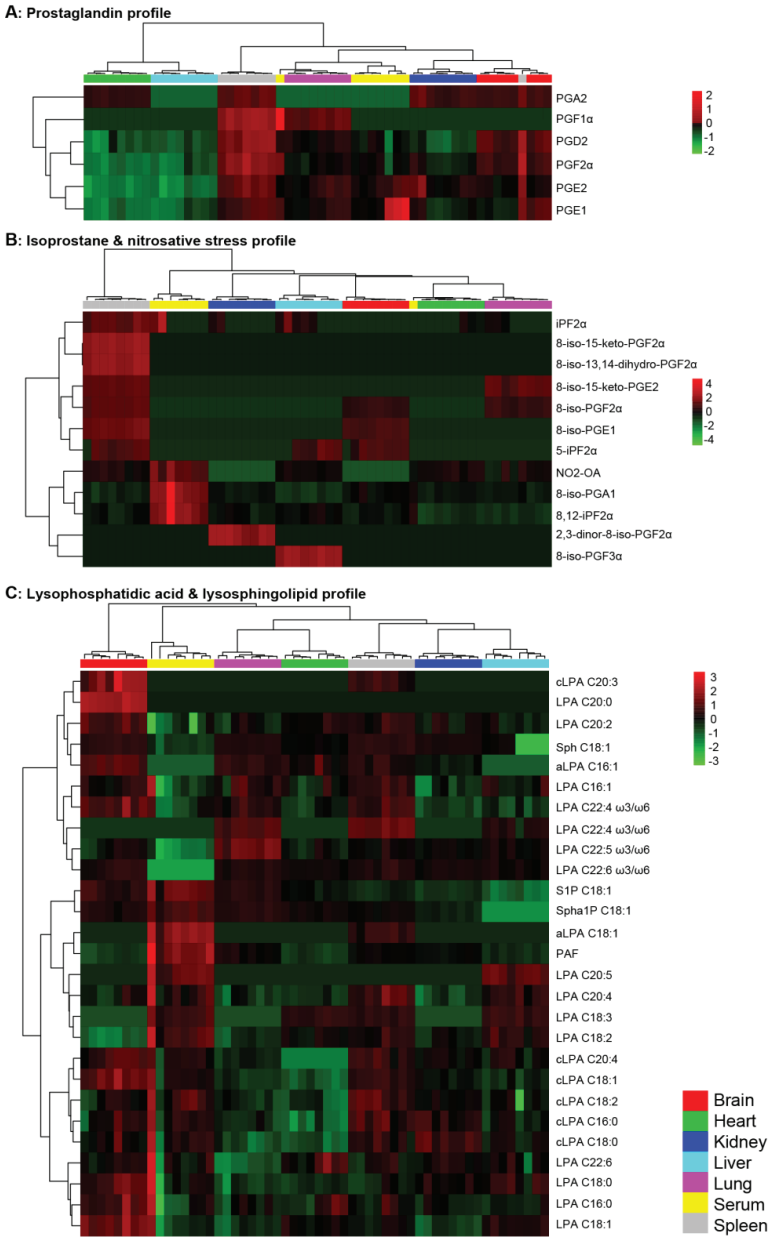

Figure 2.5. Heatmaps of all detected metabolites divided into A – Prostaglandins, B – Isoprostanes and Nitro-Fatty acids and C – Lysophosphatidic acids and lysosphingolipids using Euclidean distance measure and Ward clustering algorithm.

First, we investigated the prostaglandin profile (Figure 2.5 A), and found that the spleen has the highest level of prostaglandins present. Interestingly, the brain also shows high prostaglandin levels even with the reduced extraction efficiency, with PGD_2 and $PGF_{2\alpha}$ being the dominant species. Both the heart and liver samples have the lowest levels detected for the prostaglandins. The kidney samples have high levels of especially PGE_2 and PGA_2, and the lung has high levels of $PGF_{1\alpha}$. The reasons for these unique prostaglandin profiles could be attributed to their signalling functioning, and its relation to the specific tissue function. The spleen is an interface between the circulating blood and lymph systems critical for innate and adaptive immune responses, especially against bacterial and fungal infections. It is also essential in regulating erythrocyte level. The presence of high levels of prostaglandins within the spleen highlights the immunological importance of these lipid mediator species in orchestrating the differentiation, migration and response of leukocytes [41,42]. High levels of PGE_2 in the kidney relates to its homeostatic role in fluid metabolism and hemodynamic effects. PGE_2 regulates blood flow in the kidney and sodium excretion influencing blood pressure [43–45]. PGD_2 has been identified as the main central nervous system prostaglandin in rats, functioning in a protective nature [46,47]. The low levels of prostaglandins detected in the heart and liver possibly reflect the healthy status of these animals. Serum prostaglandin readouts were quite diverse with some samples presenting especially high levels of PGE_1 (and to a lesser extent PGE_2) while other samples had much lower levels. Even though these mice present baseline levels, some physiological state cannot be excluded, and the differences found might be subtle, or important!?

Next we zoomed in on the homeostatic stress-related lipid-profile consisting of the isoprostanes and NO_2-FAs (Figure 2.5 B). Interestingly, the most characterised and described isoprostane, 8-iso-$PGF_{2\alpha}$ was only detected in brain, lung and spleen tissues, whereas the isoprostane 8,12-iso-$iPF_{2\alpha}$ IV was detected in all six tissues and serum, and might be a more sensitive readout for oxidative stress. The downstream metabolite of 8-iso-$PGF_{2\alpha}$, 2,3-dinor-8-iso-$PGF_{2\alpha}$, was strongly detected within serum and kidney tissue, revealing the metabolising and excretion of oxidative stress markers via urine. Nitro-oleic acid, was detected in all tissues and serum except for brain, heart and kidney. In work published by Fu et al, urine provides an excellent sample matrix for assessing the levels of NO_2-FAs [48]. Overall, the spleen presented the highest levels of oxidative stress markers. It is interesting to note that the different tissues all had different types of isoprostanes present. As lipid oxidation and nitration via ROS and RNS is a non-enzymatic, non-specific process, the homeostatic levels possibly are reflective of low-level stress and redox biology processes and that this are to some extent probably tissue function related.

Lastly, we focused on the lysophosphatidic acids and lyso-sphingolipids (Figure 2.5 C). The brain is a rich source of lysophosphatic acid as well as the spleen. Lysophosphatidic acid has been found to have its highest levels in brain tissues compared to the liver, lung and heart in rats [49]. The function of lysophosphatidic acid within the spleen relates to its ability to induce chemokines in T cells, regulating its migration to secondary lymphoid tissues [50]. S1P and Spha1P presented with high levels detected within the serum and lower levels within the tissues samples, whereas sphingosine and sphinganine had lowered serum levels compared to higher tissue levels. This S1P gradient supports the vascular function of S1P, important in endothelial barrier integrity via its G-protein-coupled S1P receptor-1 [51,52]. Within tissues, the synthesis of S1P is dependent on sphingosine levels after which S1P is either excreted or metabolised. Even though the spleen is a rich source of blood, the signalling capacity of S1P within the spleen is of critical importance to the migration of B cells and T cells.

Ramos-Perez et al found in an elegant study done that the spleen has exquisitely tight regulation of S1P levels and that the level of S1P in the spleen was very low compared to the circulating plasma [53].

Serum provides a non-tissue specific homeostatic stress and inflammation readout

As shown above, each tissue clearly has a distinct homeostatic metabolic stress and inflammatory profile primarily related to tissue function, therefore it is interesting to determine how reflective serum is as a systemic readout of these different tissue profiles. Due to the relative ease and non-invasive collection protocols for most bio-fluids (serum, plasma and urine), they are frequently the sample material of choice in studies investigating health and disease, although a possible drawback of bio-fluids is that they represent a systemic readout of a highly dynamic system rather than allowing tissue specific readouts. For the metabolites studied in this method it is still rather unclear whether the serum profile reflects the physiology of the various tissues, as its difficult to determine the origins of most metabolites within serum. It is generally believed that localised disease perturbations within the body are severe enough to spill over into the circulation, where it can be measured in a less invasive manner. This is also the fundamental principal in disease biomarker studies, where systemic circulating metabolites are sensitive and specific for a particular disease, acting as a biomarker (bio-signature or disease fingerprint) [54,55]. However, when doing biological investigations into the pathogenic mechanism governing diseases, it is debatable whether we can draw correct conclusions using a systemic readout only. Due to the paired nature of the samples used, we performed spearman correlation analyses between the same metabolites in the different tissues and serum samples, revealing an interesting picture resulting in both positive and negative correlations (Table 2.2).

Table 2.2 Spearman correlation analyses of paired tissue and serum samples. All correlations have a $p < 0.05$ and the correlation coefficient are shown with its corresponding metabolite.

	Spleen	Lung	Liver	Kidney	Heart	Brain	Serum
Spleen							
Lung	cLPA C18:2 (-0.833)						
Liver	cLPA C18:2 (-0.881)	8,12-iPF$_{2\alpha}$ VI (-0.81) LPA C18:1 (-0.786) cLPA C18:2 (0.786) cLPA C18:1 (0.833) PAF (0.952)					
Kidney	8-iso-PGA$_1$ (-0.738)	LPA C16:1 (0.714)					
Heart		PGE$_1$ (0.714) LPA C18:0 (0.762) cLPA C18:1 (-0.81)		PGF$_{2\alpha}$ (0.762) S1P (0.714) LPA C18:0 (0.786) cLPA C16:0 (0.881)			
Brain	5-iPF$_{2\alpha}$ VI (0.857) LPA C18:2 (-0.905) LPA C20:4 (-0.738) LPA C22:4 (-0.738) LPA C20:2 (-0.762)			LPA C16:1 (0.81) LPA C18:0 (-0.905)	8-iso-PGA$_1$ (0.952) LPA C18:0 (-0.738)		
Serum	PGD$_2$ (0.857) LPA C20:2 (0.743) cLPA C18:1 (-0.738)			8,12-iPF$_{2\alpha}$ VI (0.952)	LPA C16:1 (-0.738)		

Three metabolites correlated significantly between serum and spleen tissue and one correlation was found each for kidney and heart tissues; interestingly, these were all different metabolites. Urade et al. reported that the major source of endogenous PGD$_2$ derived from a glutathione dependant prostaglandin D2 synthase are produced by antigen presenting cells, of which the spleen is a rich source under homeostasis, supporting this finding [56]. The isoprostane 8,12-iPF$_{2\alpha}$-VI correlated strongly between serum and kidney tissue samples, alluding to the excretion of these metabolites via urine. Interestingly, both positive and negative lysophosphatidic acid correlations are observed between the different tissues, of which the interpretation remains unclear. Especially spleen and brain tissue indicated a strong correlation with four unsaturated lysophosphatidic acid species identified as significantly negatively correlated.

Taken collectively, few correlations were found between circulating serum and tissue metabolism when investigating the baseline stress and inflammatory profiles of healthy animals. Furthermore, the subtle correlations could allude to organ regulation of signalling metabolites as well as intra-organ metabolic compartmentalisation. It's quite well known that different organs are comprised of different tissue subtypes. For example, the spleen consists of white and red pulp with each having unique properties, functions and quite possibly also metabolism. Thus, when studying metabolic questions related to health and disease choosing the proper sample material is of critical importance to accurately reflect the investigated pathological condition.

Conclusion

As oxidative stress and inflammation are central to many known diseases, the development of a method able to provide systemic and localised readouts is of the utmost importance. In addition, in some tissues and some diseases nitrosative stress is an important process. The developed and validated methodology provides a stress readout based on the isoprostanes and NO_2-FAs reflective of lipid peroxidation and nitration, as well as an inflammatory readout based on the prostaglandins, LPAs and LSLs. Application of this methodology to biological questions related to health and disease will broaden our understanding of oxidative stress and inflammation on the metabolic level. The application of this metabolomics profiling method to healthy mice found that the systemic (serum profile) readout for stress and inflammation markers was hardly correlating with the profiles in the six tested tissues at baseline conditions. Although, we did identify serum metabolites correlating with levels in the spleen, heart and kidney as well as significant tissue-tissue metabolic correlations. In addition, each tissue type presented a unique homeostatic stress and inflammation profile. This might be due to the tightly controlled nature of these potent biological signalling lipids during homeostasis. In the event of a severe health perturbation, the reflective nature of this panel of metabolites in serum needs to be evaluated as the localised perturbation can spill over into a system readout, while also affecting other tissues and organs.

Acknowledgements

This study was supported by the NWO-ZonMW grant number 435002027, and the Virgo consortium, funded by the Dutch government project number FES0908. We would also like to thank Shimadzu for the use of the LCMS-8050, as well as their technical advice and services.

References

1. Sundaresan, M., Yu, Z. X., Ferrans, V. J., Irani, K. & Finkel, T. Requirement for generation of H2O2 for platelet-derived growth factor signal transduction. *Science* **270,** 296–9 (1995).
2. Denu, J. M. & Tanner, K. G. Specific and reversible inactivation of protein tyrosine phosphatases by hydrogen peroxide: evidence for a sulfenic acid intermediate and implications for redox regulation. *Biochemistry* **37,** 5633–42 (1998).
3. Al-Mehdi, A.-B. *et al.* Perinuclear mitochondrial clustering creates an oxidant-rich nuclear domain required for hypoxia-induced transcription. *Sci. Signal.* **5,** ra47 (2012).
4. Winterbourn, C. C. & Hampton, M. B. Thiol chemistry and specificity in redox signaling. *Free Radic. Biol. Med.* **45,** 549–61 (2008).
5. Finkel, T. From sulfenylation to sulfhydration: what a thiolate needs to tolerate. *Sci. Signal.* **5,** pe10 (2012).
6. Dizdaroglu, M. & Jaruga, P. Mechanisms of free radical-induced damage to DNA. *Free Radic. Res.* **46,** 382–419 (2012).
7. Federico, A., Morgillo, F., Tuccillo, C., Ciardiello, F. & Loguercio, C. Chronic inflammation and oxidative stress in human carcinogenesis. *Int. J. cancer* **121,** 2381–6 (2007).
8. Bauer, M. E. & Fuente, M. D. la. The role of oxidative and inflammatory stress and persistent viral infections in immunosenescence. *Mech. Ageing Dev.* 1–11 (2016). doi:10.1016/j.mad.2016.01.001
9. Hybertson, B. M., Gao, B., Bose, S. K. & McCord, J. M. Oxidative stress in health and disease: the therapeutic potential of Nrf2 activation. *Mol. Aspects Med.* **32,** 234–46 (2011).

10. Uttara, B., Singh, A. V, Zamboni, P. & Mahajan, R. T. Oxidative stress and neurodegenerative diseases: a review of upstream and downstream antioxidant therapeutic options. *Curr. Neuropharmacol.* **7,** 65–74 (2009).
11. Schieber, M. & Chandel, N. S. ROS function in redox signaling and oxidative stress. *Curr. Biol.* **24,** R453–R462 (2014).
12. Mattson, M. P. Hormesis defined. *Ageing Res. Rev.* **7,** 1–7 (2008).
13. Bielski, B. H., Arudi, R. L. & Sutherland, M. W. A study of the reactivity of HO2/O2- with unsaturated fatty acids. *J. Biol. Chem.* **258,** 4759–61 (1983).
14. Spiteller, G. Are lipid peroxidation processes induced by changes in the cell wall structure and how are these processes connected with diseases? *Med. Hypotheses* **60,** 69–83 (2003).
15. Roberts, L. J. & Milne, G. L. Isoprostanes. *J. Lipid Res.* **50 Suppl,** S219–23 (2009).
16. Rokach, J. *et al.* Total synthesis of isoprostanes: discovery and quantitation in biological systems. *Chem. Phys. Lipids* **128,** 35–56 (2004).
17. Baker, P. R. S., Schopfer, F. J., O'Donnell, V. B. & Freeman, B. a. Convergence of nitric oxide and lipid signaling: anti-inflammatory nitro-fatty acids. *Free Radic. Biol. Med.* **46,** 989–1003 (2009).
18. Moore, C. B. & Ting, J. P.-Y. Regulation of mitochondrial antiviral signaling pathways. *Immunity* **28,** 735–9 (2008).
19. West, A. P. *et al.* TLR signalling augments macrophage bactericidal activity through mitochondrial ROS. *Nature* **472,** 476–80 (2011).
20. Kalinski, P. Regulation of immune responses by prostaglandin E2. *J. Immunol. (Baltimore, Md 1950)* **188,** 21–28 (2012).
21. Ricciotti, E. & FitzGerald, G. A. Prostaglandins and Inflammation. *Arterioscler. Thromb. Vasc. Biol.* **31,** 986–1000 (2011).
22. Spiegel, S. & Milstien, S. The outs and the ins of sphingosine-1-phosphate in immunity. *Nat. Rev. Immunol.* **11,** 403–15 (2011).
23. Peng, X. *et al.* Protective effects of sphingosine 1-phosphate in murine endotoxin-induced inflammatory lung injury. *Am. J. Respir. Crit. Care Med.* **169,** 1245–51 (2004).
24. Allende, M. L., Dreier, J. L., Mandala, S. & Proia, R. L. Expression of the Sphingosine 1-Phosphate Receptor, S1P1, on T-cells Controls Thymic Emigration. *J. Biol. Chem.* **279,** 15396–15401 (2004).
25. Maceyka, M. & Spiegel, S. Sphingolipid metabolites in inflammatory disease. *Nature* **510,** 58–67 (2014).
26. Lin, C.-I. *et al.* Lysophosphatidic acid regulates inflammation-related genes in human endothelial cells through LPA1 and LPA3. *Biochem. Biophys. Res. Commun.* **363,** 1001–8 (2007).
27. Fujiwara, Y. Cyclic phosphatidic acid - a unique bioactive phospholipid. *Biochim. Biophys. Acta* **1781,** 519–24 (2008).
28. Ramautar, R., Berger, R., van der Greef, J. & Hankemeier, T. Human metabolomics: strategies to understand biology. *Curr. Opin. Chem. Biol.* **17,** 841–846 (2013).
29. Xiao, J. F., Zhou, B. & Ressom, H. W. Metabolite identification and quantitation in LC-MS/MS-based metabolomics. *Trends Analyt. Chem.* **32,** 1–14 (2012).
30. Wolfer, A. M., Gaudin, M., Taylor-Robinson, S. D., Holmes, E. & Nicholson, J. K. Development and Validation of a High-Throughput Ultrahigh-Performance Liquid Chromatography–Mass Spectrometry Approach for Screening of Oxylipins and Their Precursors. *Anal. Chem.* **87,** 11721–11731 (2015).
31. Xia, J., Sinelnikov, I. V., Han, B. & Wishart, D. S. MetaboAnalyst 3.0—making metabolomics more meaningful. *Nucleic Acids Res.* **43,** W251–W257 (2015).

32. Tsikas, D., Zoerner, A. a, Mitschke, A. & Gutzki, F.-M. Nitro-fatty acids occur in human plasma in the picomolar range: a targeted nitro-lipidomics GC-MS/MS study. *Lipids* **44,** 855–65 (2009).
33. Quehenberger, O. *et al.* Lipidomics reveals a remarkable diversity of lipids in human plasma. *J. Lipid Res.* **51,** 3299–305 (2010).
34. Ohkawa, R. *et al.* Plasma sphingosine-1-phosphate measurement in healthy subjects: close correlation with red blood cell parameters. *Ann. Clin. Biochem.* **45,** 356–63 (2008).
35. Onorato, J. M. *et al.* Challenges in accurate quantitation of lysophosphatidic acids in human biofluids. *J. Lipid Res.* **55,** 1784–1796 (2014).
36. Zhao, Z. & Xu, Y. Measurement of endogenous lysophosphatidic acid by ESI-MS/MS in plasma samples requires pre-separation of lysophosphatidylcholine. *J. Chromatogr. B. Analyt. Technol. Biomed. Life Sci.* **877,** 3739–42 (2009).
37. Scherer, M., Leuthäuser-Jaschinski, K., Ecker, J., Schmitz, G. & Liebisch, G. A rapid and quantitative LC-MS/MS method to profile sphingolipids. *J. Lipid Res.* **51,** 2001–11 (2010).
38. FDA, F. and D. A. Guidance for industry. Bioanalytical method validation. *U.S. Dep. Heal. Hum. Serv.* (2013). at <http://www.fda.gov/downloads/drugs/guidancecomplianceregulatoryinformation/guidances/ucm368107.pdf>
39. Administration, F. and D. *Guidance for Industry: Bioanalytical method validation. U.S. Department of Health and Human Services* (2001). doi:http://www.labcompliance.de/documents/FDA/FDA-Others/Laboratory/f-507-bioanalytical-4252fnl.pdf
40. Alves, R. D. A. M. *et al.* Global profiling of the muscle metabolome: method optimization, validation and application to determine exercise-induced metabolic effects. *Metabolomics* **11,** 271–285 (2015).
41. Kim, N. & Luster, A. D. Regulation of immune cells by eicosanoid receptors. *ScientificWorldJournal.* **7,** 1307–1328 (2007).
42. Norris, P. C. & Dennis, E. A. A lipidomic perspective on inflammatory macrophage eicosanoid signaling. *Adv. Biol. Regul.* **54,** 99–110 (2014).
43. Villa, E., Garcia-Robles, R., Haas, J. & Romero, J. C. Comparative effect of PGE2 and PGI2 on renal function. *Hypertension* **30,** 664–6 (1997).
44. Long, C. R., Kinoshita, Y. & Knox, F. G. Prostaglandin E2 induced changes in renal blood flow, renal interstitial hydrostatic pressure and sodium excretion in the rat. *Prostaglandins* **40,** 591–601 (1990).
45. Jia, Z. *et al.* Role of COX-2/mPGES-1/prostaglandin E2 cascade in kidney injury. *Mediators Inflamm.* **2015,** 147894 (2015).
46. Abdel-Halim, M. S., Hamberg, M., Sjöquist, B. & Ångård, E. Identification of prostaglandin D2 as a major prostaglandin in homogenates of rat brain. *Prostaglandins* **14,** 633–643 (1977).
47. Narumiya, S., Ogorochi, T., Nakao, K. & Hayaishi, O. Prostaglandin D2 in rat brain, spinal cord and pituitary: Basal level and regional distribution. *Life Sci.* **31,** 2093–2103 (1982).
48. Fu, J. *et al.* Metabolomics profiling of the free and total oxidised lipids in urine by LC-MS/MS: application in patients with rheumatoid arthritis. *Anal. Bioanal. Chem.* (2016). doi:10.1007/s00216-016-9742-2
49. Das, A. K. & Hajra, A. K. Quantification, characterization and fatty acid composition of lysophosphatidic acid in different rat tissues. *Lipids* **24,** 329–33 (1989).
50. Kanda, H. *et al.* Autotaxin, an ectoenzyme that produces lysophosphatidic acid, promotes the entry of lymphocytes into secondary lymphoid organs. *Nat. Immunol.* **9,** 415–23 (2008).

51. Adamson, R. H. *et al.* Sphingosine-1-phosphate modulation of basal permeability and acute inflammatory responses in rat venular microvessels. *Cardiovasc. Res.* **88,** 344–51 (2010).
52. Jung, B. *et al.* Flow-regulated endothelial S1P receptor-1 signaling sustains vascular development. *Dev. Cell* **23,** 600–10 (2012).
53. Ramos-Perez, W. D., Fang, V., Escalante-Alcalde, D., Cammer, M. & Schwab, S. R. A map of the distribution of sphingosine 1-phosphate in the spleen. *Nat. Immunol.* **16,** 1245–52 (2015).
54. Serkova, N. J., Standiford, T. J. & Stringer, K. A. The emerging field of quantitative blood metabolomics for biomarker discovery in critical illnesses. *Am. J. Respir. Crit. Care Med.* **184,** 647–55 (2011).
55. Xia, J., Broadhurst, D. I., Wilson, M. & Wishart, D. S. Translational biomarker discovery in clinical metabolomics: An introductory tutorial. *Metabolomics* **9,** 280–299 (2013).
56. Urade, Y., Ujihara, M., Horiguchi, Y., Ikai, K. & Hayaishi, O. The major source of endogenous prostaglandin D2 production is likely antigen-presenting cells. Localization of glutathione-requiring prostaglandin D synthetase in histiocytes, dendritic, and Kupffer cells in various rat tissues. *J. Immunol.* **143,** 2982–9 (1989).

Supplementary information

Supplementary Tables

Table S2.1 Provides an over view of the calibration solution and spiked levels used during this study

Calibration level	Stock concentration (nM)	dilution factor based on C8 level	Calibration level when spiked into 150 uL samples (nM)
C8	1304	-	156
C7	1000	0.77	120
C6 (high)	500	0.38	60
C5	250	0.19	30
C4 (Medium)	100	0.08	12
C3	10	0.0077	1.2
C2 (Low)	2.5	0.0019	0.3
C1	0.75	0.00058	0.09
C0	0	0	0

Table S2.2: Target list with optimised MRM transitions for the identified metabolites, putative identified metabolites and ISTDs.

Compound class	Compound name	Precursor ion> Product ion (m/z)	CE (V)	Dwell time (msec)	MS Polarity	Internal standard	Lipid Maps ID
Identified metabolites based on standards							
Alkyl-lyso-phosphatidic acid *	aLPA C18:1	421.20>78.95	26	12	Neg	LPA C17:0	x
Cyclic-lyso-phosphatidic acid *	cLPA C18:1	417.20>281.00	17	12	Neg	cLPA C17:0	LMGP00000056
Isoprostane	2,3-dinor-11B-iso-PGF2α	325.00>145.20	20	20	Neg	(d4) PGF2α	LMFA03010011
Isoprostane	2,3-dinor-8-iso-PGF2α	325.10>237.20	12	20	Neg	(d4) 8-iso-PGF2α	LMFA03110010
Isoprostane	5-iPF2α VI	353.30>115.05	22	40	Neg	(d11) 5-iPF2α VI	LMFA03110010
Isoprostane	8,12-iPF2α VI	353.30>115.05	22	40	Neg	(d11) 8,12-iPF2α VI	
Isoprostane	8-iso-13,14-dihydro-PGF2α	353.30>183.10	25	20	Neg	(d4) 8-iso-PGF2α	
Isoprostane	8-iso-15-keto-PGE2	349.10>287.20	16	20	Neg	(d4) 8-iso-PGE2	LMFA03110009
Isoprostane	8-iso-15-keto-PGF2α	351.10>315.15	22	20	Neg	(d4) 8-iso-PGF2α	LMFA03110005
Isoprostane	8-iso-15-keto-PGF2b	351.10>315.15	22	20	Neg	(d4) 8-iso-PGF2α	
Isoprostane	8-iso-15-R-PGF2α	353.30>193.20	25	20	Neg	(d4) 8-iso-PGF2α	
Isoprostane	8-iso-PGA1	335.10>273.15	19	20	Neg	(d4) PGA2	LMFA03110008
Isoprostane	8-iso-PGA2	333.10>271.20	15	20	Neg	(d4) PGA2	
Isoprostane	8-iso-PGE1	353.30>317.20	15	20	Neg	(d4) PGE1	LMFA03110002
Isoprostane	8-iso-PGE2	351.10>271.15	17	20	Neg	(d4) 8-iso-PGE2	LMFA03110003
Isoprostane	8-iso-PGF1α	355.30>311.10	22	20	Neg	(d9) 8-iso-PGF1α	
Isoprostane	8-iso-PGF2α (15-F2t-IsoP)	353.30>193.20	25	20	Neg	(d4) 8-iso-PGF2α	LMFA03110001
Isoprostane	8-iso-PGF3α	351.10>307.15	19	20	Neg	(d4) 8-iso-PGF2α	LMFA03110007
Isoprostane	iPFa-IV	353.30>127.10	22	20	Neg	(d4) iPFa-VI	
Lyso-phosphatidic acid *	LPA C16	409.00>153.05	22	12	Neg	LPA C17:0	LMGP10050006
Lyso-phosphatidic acid *	LPA C18	437.30>153.05	24	12	Neg	LPA C17:0	LMGP10050005
Lyso-phosphatidic acid *	LPA C20:4	456.70>153.05	22	12	Neg	LPA C17:0	LMGP10050013
Lyso-sphingolipid	SPH C18:1	300.10>252.30	-18	8	Pos	Sph C17:1	LMSP01010001
Lyso-sphingolipid	SPHA C18:0	302.50>60.05	-22	8	Pos	Spha C17:0	LMSP01020001
Lyso-sphingolipid *	SPHA-1-P C18:0	380.00>79.05	41	12	Neg	Spha-1-P C17:0	LMSP01050002
Lyso-sphingolipid *	S1P C18 :1	378.00>79.05	25	12	Neg	Sph-1-P C17:1	LMSP01050001
Nitro-Fatty acid	NO2-LA (C18:2)	324.30>277.25	12	40	Neg	10-Nitrooleate-d17	LMFA01120001/2
Nitro-Fatty acid	NO2-OA (C18:1)	326.10>46.00	14	40	Neg	10-Nitrooleate-d17	LMFA01120003/4
Platelet activating factor *	PAF C16:0	524.20>125.10	-25	15	Pos	PAF C18:0-d4	LMGP01020046
Prostaglandins	13,14-dihydro-PGF2α	353.30>183.10	25	20	Neg	(d4) PGF2α	LMFA03010079
Prostaglandins	PGA1	335.10>273.15	19	20	Neg	(d4) PGA2	LMFA03010005
Prostaglandins	PGA2	333.10>271.20	15	20	Neg	(d4) PGA2	LMFA03010035
Prostaglandins	PGD2	351.10>271.15	17	20	Neg	(d4) PGD2	LMFA03010004
Prostaglandins	PGD3	349.10>269.20	17	20	Neg	(d4) PGD2	LMFA03010142
Prostaglandins	PGE1	353.30>317.20	15	20	Neg	(d4) PGE1	LMFA03010134
Prostaglandins	PGE2	351.10>271.15	17	20	Neg	(d9) PGE2	LMFA03010003
Prostaglandins	PGE3	349.10>269.20	17	20	Neg	(d9) PGE2	LMFA03010135
Prostaglandins	PGF1α	355.30>311.10	22	20	Neg	(d9) 8-iso-PGF1α	LMFA03010137
Prostaglandins	PGF2α	353.30>193.20	25	20	Neg	(d4) PGF2α	LMFA03010002
Prostaglandins	PGF3α	351.10>307.15	19	20	Neg	(d4) PGF2α	LMFA03010138

Putatively identified metabolites							
Alkyl-lyso-phosphatidic acid *	aLPA C16:1	393.20>78.95	25	12	Neg	LPA C17:0	x
Cyclic-lyso-phosphatidic acid *	cLPA C16:0	390.90>255.00	20	12	Neg	cLPA C17:0	LMGP00000057
Cyclic-lyso-phosphatidic acid *	cLPA C18:0	418.90>283.00	20	12	Neg	cLPA C17:0	LMGP00000055
Cyclic-lyso-phosphatidic acid *	cLPA C18:2	414.90>279.00	20	12	Neg	cLPA C17:0	x
Cyclic-lyso-phosphatidic acid *	cLPA C20:3	440.90>305.00	20	12	Neg	cLPA C17:0	x
Cyclic-lyso-phosphatidic acid *	cLPA C20:4	438.90>303.00	20	12	Neg	cLPA C17:0	x
Lyso-phosphatidic acid *	LPA C14:0	381.20>153.05	22	12	Neg	LPA C17:0	LMGP10050007
Lyso-phosphatidic acid *	LPA C16:1	407.20>153.05	22	12	Neg	LPA C17:0	LMGP10050016
Lyso-phosphatidic acid *	LPA C18:1	435.20>153.05	22	12	Neg	LPA C17:0	LMGP10050008
Lyso-phosphatidic acid *	LPA C18:2	433.20>153.05	22	12	Neg	LPA C17:0	LMGP10050017
Lyso-phosphatidic acid *	LPA C18:3	431.20>153.05	22	12	Neg	LPA C17:0	LMGP10050023
Lyso-phosphatidic acid *	LPA C20:0	465.20>153.05	22	12	Neg	LPA C17:0	LMGP10050018
Lyso-phosphatidic acid *	LPA C20:1	463.20>153.05	22	12	Neg	LPA C17:0	LMGP10050026
Lyso-phosphatidic acid *	LPA C20:2	461.20>153.05	22	12	Neg	LPA C17:0	LMGP10050027
Lyso-phosphatidic acid *	LPA C20:3	459.20>153.05	22	12	Neg	LPA C17:0	LMGP10050028
Lyso-phosphatidic acid *	LPA C20:5	455.20>153.05	22	12	Neg	LPA C17:0	LMGP10050033
Lyso-phosphatidic acid *	LPA C22:4	485.20>153.05	22	12	Neg	LPA C17:0	LMGP10050020
Lyso-phosphatidic acid *	LPA C22:5	483.20>153.05	22	12	Neg	LPA C17:0	x
Lyso-phosphatidic acid *	LPA C22:6	481.20>153.05	22	12	Neg	LPA C17:0	LMGP10050019
Nitro-Fatty acid	NO2-aLA (C18:3)	322.10>46.05	12	12	Neg	10-Nitrooleate-d17	
Internal standards							
Cyclic-lyso-phosphatidic acid *	cLPA C17:0	405.20>269.25	20	12	Neg	*na*	
Isoprostane	5-iPF2α-VI-d11	364.20>115.05	22	20	Neg	*na*	LMFA03110011
Isoprostane	8-iso-PGE2-d4	355.30>275.25	18	20	Neg	*na*	LMFA03010008
Isoprostane	8-iso-PGF1α-d9	364.20>320.25	23	20	Neg	*na*	
Isoprostane	8-iso-PGF2α-d4	357.30>197.15	20	20	Neg	*na*	
Isoprostane	iPF2α-VI-d4	357.20>114.90	22	20	Neg	*na*	
Isoprostane	8,12-iso-iPF2α-VI-d11	364.20>115.05	23	40	Neg	*na*	
Lyso-phosphatidic acid *	LPA C17:0	423.20>153.05	22	12	Neg	*na*	LMGP10050036
Lyso-sphingolipid	Sph C17:1	285.90>238.30	-14	8	Pos	*na*	
Lyso-sphingolipid	Spha C17:0	288.10>59.80	-18	8	Pos	*na*	
Lyso-sphingolipid *	S1P C17:1	364.00>78.95	30	12	Neg	*na*	
Lyso-sphingolipid *	Spha-1-P C17:0	366.00>79.05	28	12	Neg	*na*	
Nitro-Fatty acid	10-Nitrooleate-d17	343.10>46.05	15	20	Neg	*na*	
Platelet activating factor *	PAF C16:0-d4	527.70>125.00	-52	15	Pos	*na*	
Prostaglandins	PGD2-d4	355.30>275.25	18	20	Neg	*na*	LMFA03010007
Prostaglandins	PGF2α-d4	357.30>197.15	20	20	Neg	*na*	LMFA03010006
Prostaglandins	PGE2-d9	359.90>280.25	18	20	Neg	*na*	
Prostaglandins	PGE1-d4	357.30>321.20	15	20	Neg	*na*	
Prostaglandins	PGA2-d4	336.90>275.00	11	20	Neg	*na*	
Reference	Cuda	339.30>214.25	24		Neg	*na*	

* Indicates that the metabolite is measured during the high pH run

Table S2.3: An overview of the conditions tested and each class's response in the selected setup

pH conditions	Low pH (<3.4)		High pH (10.3) (* Addition of salt)	
Organic modifier	**Methanol**	**Acetonitrile**	**Methanol**	**Acetonitrile**
Isoprostanes	Isomer separation problems	*Good*	Good *Ion suppression	Elutes too early < 20 % B
Prostaglandins	Isomer separation problems	*Good*	Good *Ion suppression	Elutes too early < 20 % B
Nitro-fatty acids	*Good*	*Good*	*Good*	*Good*
LPAs & aLPAs	Peak tailing Carry over > 20%	Peak tailing Carry over > 20%	*OK peak shape* *Carry over > 5 %* **Carry over < 3%*	*OK peak shape* *Carry over > 5 %* **Carry over < 3%*
cLPAs	*Good peak shape*	*Good peak shape*	*Good peak shape*	*Good peak shape*
S1P & Spha1P	Peak tailing Carry over > 20%	Peak tailing Carry over > 20%	*OK peak shape* *Carry over > 5 %* **Carry over < 2%*	*OK peak shape* *Carry over > 5 %* **Carry over < 2%*
Sph & Spha	*Good peak shape*	Peak tailing	Good peak shape Carry over > 5 % * Carry over > 5 % Bad Ion suppression due to LPC/PAF co-elution	Peak tailing Carry over > 5 % * Carry over > 5 %
PAF	Good peak shape but co-eluting with LPCs	Good peak shape but co-eluting with LPCs	Good peak shape but co-eluting with LPCs	*Good peak & separating from LPC*

Green/Italics: Good chromatographic performance

No shading: Chromatographic issues as indicated

* Ammonium acetate 5mM was used in mobile phase A.

Table S2.4: Methodology validation recoveries and matrix effects in serum.

		% Recovery (Matrix)					Ion suppression			Matrix effect		
		I4 - Day 1	I4 - Day 2	I4 - Day 3	Average	RSD	I2-low	I4-medium	I6-high	I2-low	I4-medium	I6-high
Lysophosphatidic acid	LPA C17:0	101.4	78.5	96.5	92.1	13.0	0.81	0.55	0.71	1.03	0.72	0.45
	cLPA C17:0	95.8	112.1	106.9	104.9	7.9	1.88	2.44	2.00	1.53	2.02	0.97
Lysosphingolipids	Sph C17:1	101.1	87.0	98.6	95.6	7.9	1.39	2.04	1.98	0.94	0.65	0.38
	S-1-P C17:1	111.3	94.8	101.7	102.6	8.0	1.92	2.22	1.60	0.89	0.78	0.90
	Spha C17:0	106.4	92.8	102.1	100.4	6.9	0.67	0.50	0.58	0.73	0.67	0.59
	Spha-1-P C17:0	105.3	109.7	122.2	112.4	7.8	1.52	0.87	0.95	1.28	1.10	0.86
Nitro Fatty acids	d17 10-O2-OA	94.1	106.2	102.3	100.9	6.1	0.31	0.31	0.28	0.25	0.26	0.34
Prostaglandins	d9-PGE2	91.6	93.7	97.4	94.2	3.1	1.23	1.00	1.14	1.16	1.13	0.81
	d4-PGE1	93.6	95.7	96.7	95.3	1.6	1.60	1.05	1.05	1.39	1.16	0.84
	d4-PGD2	95.1	94.0	95.8	95.0	0.9	1.04	0.90	1.02	1.11	1.13	0.79
	d4-PGF2α	93.6	97.3	95.5	95.5	1.9	1.02	0.97	1.03	1.00	1.11	0.80
	d4-PGA2	96.0	98.4	96.3	96.9	1.3	1.06	0.95	0.97	0.94	1.08	0.78
Isoprostanes	d9-8-iso-PGF1α	106.5	100.2	97.7	101.5	4.4	1.04	0.86	1.00	1.30	1.35	0.96
	d4-8-iso-PGF2α	100.0	97.1	97.5	98.2	1.5	1.03	0.83	0.97	1.26	1.33	0.93
	d4-8-iso-PGE2	95.9	95.8	96.6	96.1	0.4	1.08	0.89	0.99	1.30	1.30	0.91
	d11- + 5-iPF2α VI	97.5	90.6	93.5	93.9	3.7	1.27	0.97	1.04	1.18	1.16	0.81
	d4-iPF2α VI	101.1	93.6	94.5	96.4	4.2	0.72	0.63	0.66	0.74	0.74	0.58
	d11-8,12-iPF2α VI	96.3	92.8	92.9	94.0	2.1	0.64	0.54	0.60	0.75	0.71	0.54

Table S2.5: Six different tissue validation recoveries and matrix effect results

		% Recoveries						% Matrix effect					
		Kidney	**Spleen**	**Liver**	**Lung**	**Heart**	**Brain**	**Kidney**	**Spleen**	**Liver**	**Lung**	**Heart**	**Brain**
Lysophosphatidic acid	LPA C17_0	78.5	97	70.8	75.7	105.2	52.6	0.63	0.78	0.80	0.49	0.65	0.47
	cLPA C17_0	89.2	72.1	100.8	91.4	98.9	60.8	0.54	0.66	0.53	0.42	0.87	0.31
Lysosphingolipids	Sph C17_1	112.5	96.6	103.2	103.5	86.6	81.3	0.95	0.94	1.22	0.64	0.61	0.43
	S-1-P C17_1	90.5	110.4	83	74.6	109.2	69.5	0.55	0.67	0.67	0.46	0.70	0.40
	Spha C17_0	109.0	102.7	101.2	137.9	121.0	71.5	0.37	0.42	0.40	0.27	0.37	0.14
Nitro Fatty acids	d17 10-NO2-OA	43.0	49.9	53.9	37.7	*ND*	37.8	0.40	0.29	0.29	0.26	0.43	0.28
Prostaglandins	d9-PGE2	121.3	106.3	80.7	95.9	88.8	61.0	1.04	1.07	0.96	0.68	1.00	0.58
	d4-PGE1	119.6	102.7	85.4	96.5	84.1	59.8	1.01	1.04	0.67	0.66	0.99	0.58
	d4-PGD2	113.0	95.7	75.6	94.1	85.3	57.7	1.04	1.07	0.92	0.73	1.02	0.61
	d4-PGF2α	113.7	99.9	75.3	96.4	84.4	57.7	1.00	1.02	0.75	0.65	0.98	0.53
	d4-PGA2	60.4	46.2	11.2	30.3	48.3	29.3	0.57	0.48	0.14	0.24	0.56	0.28
Isoprostanes	d9-8-iso-PGF1α	125.9	121.0	70.4	99.1	95.7	53.9	1.01	1.00	0.79	0.64	0.94	0.48
	d4-8-iso-PGF2α	118.4	105.5	65.9	102.0	87.9	55.7	0.98	1.00	0.79	0.65	0.98	0.52
	d4-8-iso-PGE2	111.1	97.7	62.4	92.3	83.5	57.8	1.01	1.04	0.56	0.66	0.96	0.56
	d11- + 5-iPF2α VI	128.6	93.9	80.0	105.7	94.5	54.7	1.23	1.11	0.93	0.78	1.07	0.62
	d4-iPF2α VI	119.9	97.2	77.1	99.5	94.1	56.5	1.27	1.16	0.94	0.82	1.10	0.66
	d11-8,12-iPF2α VI	110.0	90.0	94.7	102.2	88.9	58.5	1.23	1.13	1.22	0.80	1.06	0.70

ND: Not detected

Table S2.6 Intraday precision RSD values of the metabolites spiked to the different tissues

		Tissue Intraday precision (% RSD, n = 4)					
Class	**Metabolites**	**Spleen**	**Lung**	**Liver**	**Kidney**	**Heart**	**Brain**
Isoprostanes	2,3-dinor-8-iso-PGF2α	5.8	2.9	11.9	5.3	4.5	9.1
	8-iso-PGF3α	4.7	7.3	13.5	2.0	5.5	8.9
	2,3-dinor-11b-PGF$_{2α}$	2.8	4.1	19.2	2.7	1.9	7.5
	8-iso-15-keto-PGF2b	4.2	6.5	10.3	2.4	4.3	5.4
	8-iso-15-keto-PGE2	4.5	9.3	10.9	4.6	2.1	4.9
	8-iso-15-keto-PGF2α	3.9	9.6	11.2	3.8	4.2	5.2
	iPF2α	3.2	2.1	5.5	2.02	1.9	6.0
	8-iso-15(R)-PGF2α	4.6	3.5	18.2	0.6	2.8	5.2
	8-iso-PGF1α	1.6	3.9	20.6	8.0	2.2	3.3
	8-iso-13,14-dihydro-PGF2α	2.6	3.7	16.3	5.6	5.5	6.6
	8-iso-PGF2α	3.8	5.6	11.5	1.8	3.3	7.5
	8-iso-PGE2	3.1	3.5	4.2	2.7	2.2	3.6
	8-iso-PGE1	3.1	6.4	9.3	6.5	0.8	1.7
	5 iPF2α IV	3.3	2.0	16.2	3.1	3.1	5.3
	8-iso-PGA2	5.8	8.4	27.9	8.6	7.5	16.2
	8-iso-PGA1	7.0	5.4	10.7	9.4	6.4	14.8
	8,12-iPF2α VI	3.3	5.9	24.4	9.8	5.2	35.9
Lysophosphatidic acids	LPA C20:4	36.2	32.9	57.3	56.8	28.5	42.4
	LPA C16:0	32.7	19.2	16.0	46.7	41.1	33.9
	aLPA C18:1	35.4	35.4	17.9	13.6	21.0	15.7
	LPA C18:0	25.1	14.1	24.8	19.4	22.9	4.4
	cLPA C18:1	5.8	28.1	10.9	15.9	29.7	9.2
Lysosphingolipids	Sph C18:1	12.5	7.4	14.5	10.1	6.2	7.6
	Spha C18:0	25.1	27.2	26.4	29.9	20.6	25.6
	S1P C18:1	17.0	7.9	11.2	16.1	24.2	10.0
Nitro-Fatty acids	NO2-OA	3.7	15.9	4.3	9.3	13.6	7.4
	NO2-LA	10.4	31.5	15.1	14.7	13.3	11.6
Prostaglandins	PGE3	9.5	6.8	4.4	13.3	6.6	9.4
	PGD3	4.5	4.5	27.0	7.2	1.6	6.3
	PGF3α	3.6	3.0	10.8	3.4	1.0	2.0
	PGE2	6.8	6.2	14.4	6.4	5.4	8.6
	PGE1	2.4	3.6	4.3	6.7	1.2	2.0
	PGD2	6.7	5.2	3.4	2.1	2.8	7.3
	PGF1α	1.4	5.4	15.0	8.2	2.1	5.1
	PGF2α	5.2	5.5	3.4	3.0	2.4	4.2
	13,14-dihydro-PGF2α	2.0	6.5	6.0	2.9	1.2	3.5
	PGA2	1.8	1.9	5.1	2.5	6.3	7.8
	PGA1	2.4	2.5	5.5	3.5	5.5	7.7

Table S2.7 Comparison of the precision of metabolites (averaged per class) determined for technical replicates and biological replicates.

	Tissue types											
	Spleen		Lung		Liver		Kidney		Heart		Brain	
Metabolite class response	**Procedure % RSD (n = 12)**	**Biological % RSD (n = 8)**	**Procedure % RSD (n = 12)**	**Biological % RSD (n = 8)**	**Procedure % RSD (n = 12)**	**Biological % RSD (n = 8)**	**Procedure % RSD (n = 12)**	**Biological % RSD (n = 8)**	**Procedure % RSD (n = 12)**	**Biological % RSD (n = 8)**	**Procedure % RSD (n = 12)**	**Biological % RSD (n = 8)**
Isoprostanes	11.4	30.9	21.8	29.7	15.4	53.0	22.9	33.1	18.3	34.3	32.1	30.2
Prostaglandins	16.5	36.7	15.5	36.8	17.6	46.1	18.8	76.0	25.9	37.8	22.8	39.3
Nitro-fatty acids	26.7	44.5	45.0	91.4	34.7	19.1	*ND*	*ND*	28.9	33.1	*ND*	*ND*
LSL	30.7	32.7	19.1	25.0	18.7	41.5	19.8	27.6	18.9	28.7	25.0	41.6
LPA	30.6	41.9	36.5	41.0	40.3	39.1	31.3	33.6	30.2	40.8	31.5	44.2
aLPA	48.0	46.2	15.8	27.7	*ND*	*ND*	22.2	25.0	32.3	120.5	18.4	28.0
cLPA	32.3	38.9	28.8	35.1	34.4	47.9	19.2	30.1	36.3	46.8	26.8	64.2

ND - Not detected

LSL - Lysosphingolipids; LPA - Lysophosphatidic acids, aLPA - Alkyl-lysophosphatidic acids; cLPA - Cyclic-lysophosphatidic acids

Supplementary Figures

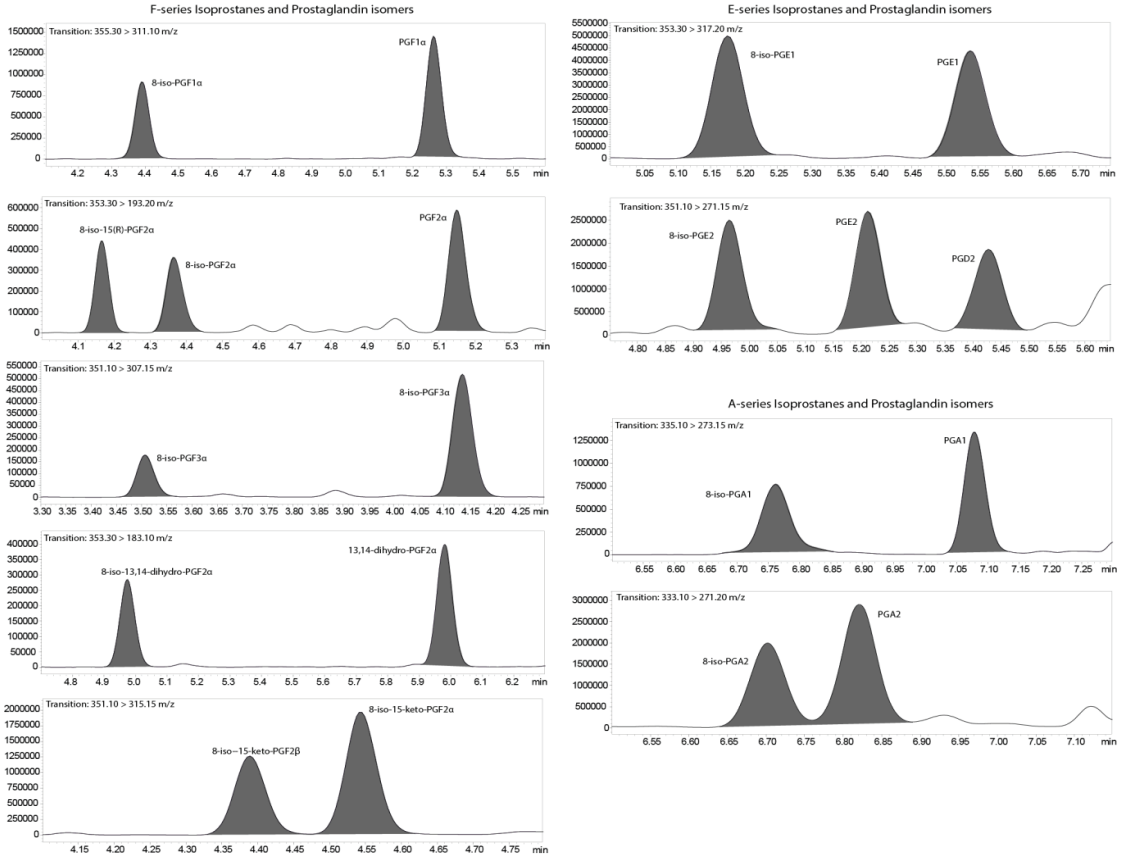

Figure S2.1 Chromatographic resolution of the different prostaglandins and isoprostanes isomers.

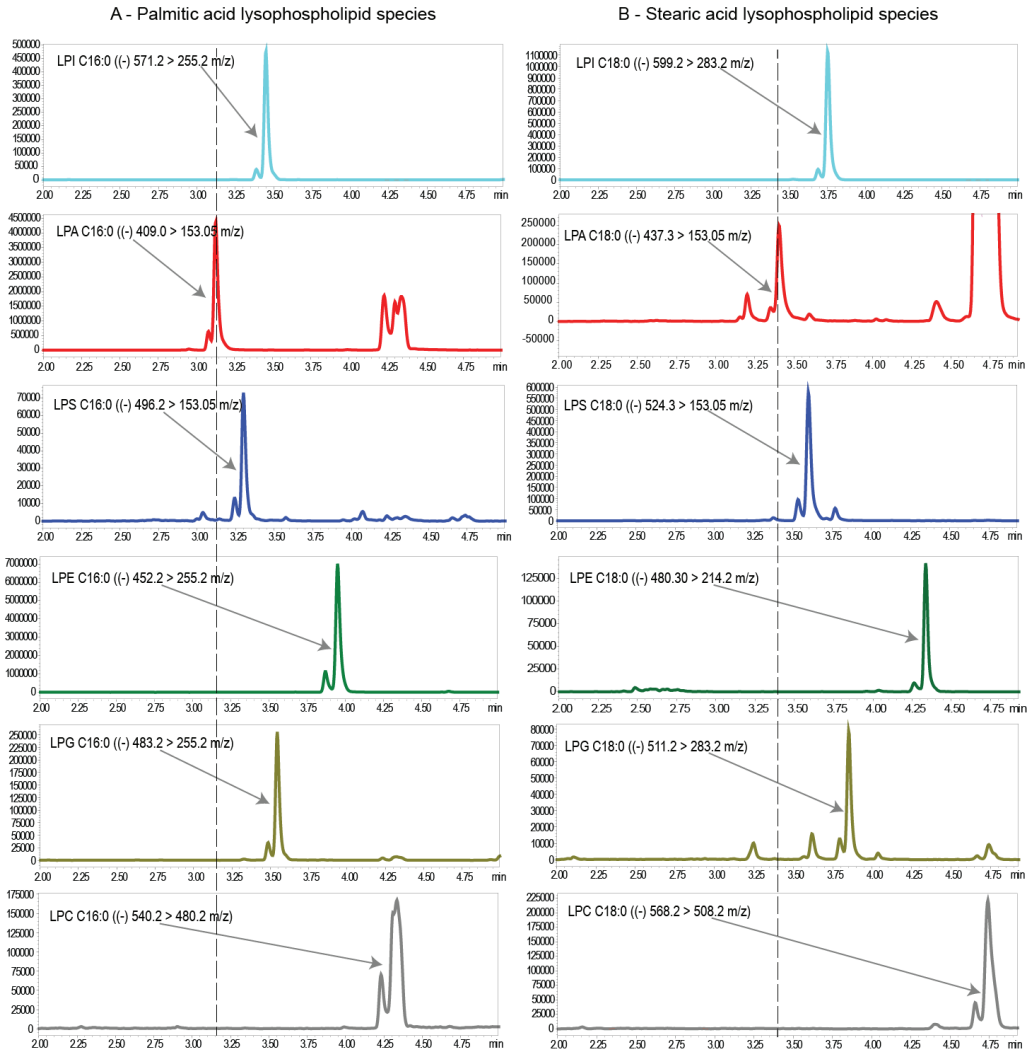

Figure S2.2: A chromatographic overview of A - palmitic acid (C16:0) and B – stearic acid (C18:0) lysophospholipid species eluting during the high pH chromatographic run. LPA elutes first for both acyl lengths followed by LPS, LPI, LPG, LPE and lastly LPC. The dashed lines indicate the retention time of the two LPA species, and no co-elution is observed for the different lysophospholipid species of the same length. LPI – Lysophosphatidylinositol; LPA – Lysophosphatidic acid; LPS – Lysophosphatidylserine; LPE – Lysophosphatidylethanolamine; LPG – Lysophosphatidylglycerol; LPC – Lysophosphatidylcholine.

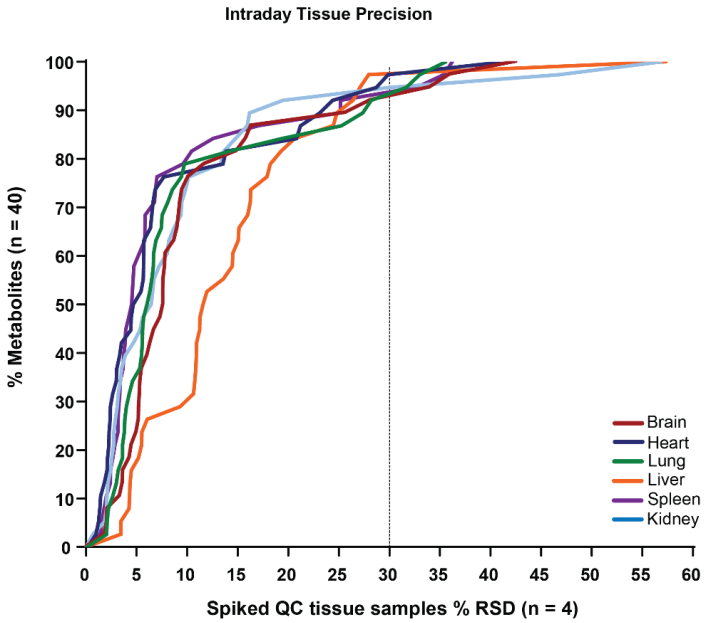

Figure S2.3: **Intraday precision in six different tissues.** Precision was determined using the RSD (n=4) of C4 spiked standards into the different tissue matrixes.

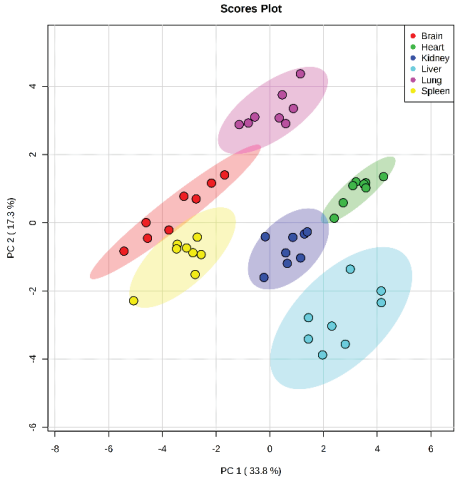

Figure S2.4 PCA analyses of the six different tissues sets, using a reduced dataset containing uniformly detected metabolites with all tissues.

Supplementary Methods

Putatively identified metabolites:

Due to the shortage of lysophosphatidic acid standards, an MS screening approach was used to putatively identify other lysophosphatidic acid species. Precursor ion scans together with single reaction monitoring (SRM) was used to search and identify putative lysophosphatidic acid species using known fragmentation patterns.

Metabolites were identified based on the following criteria:

- Retention time of putatively identified metabolites were compared to standards and had to indicate similar retention.
- Elution sequences were compared to the available standards.
    - For example, the most unsaturated acyl species of any given length eluted first followed by progressively more saturated species till the saturated one (LPA C18:3 will elute first followed by C18:2, C18:1 and lastly LPA C18:0).
- The potential lysophosphatidic acid species targeted are listed in the Table S8 below together with the calculated dehydrated parent ion's m/z.
    - Fragments monitored via SRM for lysophosphatidic acids included:
        - The dehydrated parent ion -> to the characteristic dehydrated glycerol phosphate 152.90 m/z fragment
        - The dehydrated parent ion -> to the characteristic phosphate 78.90 m/z fragment
    - Fragments monitored via SRM for cyclic-lysophosphatidic acids included:
        - The dehydrated parent ion -> to the characteristic phosphate 78.90 m/z fragment
        - The dehydrated parent ion -> to the characteristic fatty acid fragment

Subsequently, after identification putatively identified metabolites MRMs were included in the method using class the class representative commercial standards in optimizing the MS parameters.

Table S2.8: Lysophosphatidic acid and cyclic-lysophosphatidic acid species target list

Lysophosphatidic acid targets	Dehydrated parent (m/z)	Fragments		Cyclic-lysophosphatidic acid targets	Dehydrated Parent (m/z)	Fragments	
		Dehydrated glycerol phosphate (m/z)	Phosphate (m/z)			Fatty acid (m/z)	Phosphate (m/z)
LPA C14:0	381.2	152.9	78.9	cLPA C14:0	363.2	227.2	78.9
LPA C16:0 **	409.2	152.9	78.9	cLPA C16:0	391.2	255.2	78.9
LPA C16:1	407.2	152.9	78.9	cLPA C16:1	389.2	253.2	78.9
LPA C17:0 **	423.9	152.9	78.9	**cLPA C17:0 ****	405.2	269.2	78.9
LPA C18:0 **	437.2	152.9	78.9	cLPA C18:0	419.2	283.2	78.9
LPA C18:1	435.2	152.9	78.9	**cLPA C18:1 ****	417.2	281.2	78.9
LPA C18:2	433.2	152.9	78.9	cLPA C18:2	415.2	279.2	78.9
LPA C18:3	431.2	152.9	78.9	cLPA C18:3	413.2	277.2	78.9
LPA C18:4	429.2	152.9	78.9	cLPA C18:4	411.2	275.2	78.9
LPA C20:0	465.2	152.9	78.9	cLPA C20:0	447.2	311.2	78.9
LPA C20:1	463.2	152.9	78.9	cLPA C20:1	445.2	309.2	78.9
LPA C20:2	461.2	152.9	78.9	cLPA C20:2	443.2	307.2	78.9
LPA C20:3	459.2	152.9	78.9	cLPA C20:3	441.2	305.2	78.9
LPA C20:4 **	457.2	152.9	78.9	cLPA C20:4	439.2	303.2	78.9
LPA C20:5	455.2	152.9	78.9	cLPA C20:5	437.2	301.2	78.9
LPA C22:0	493.2	152.9	78.9	cLPA C22:0	475.2	339.2	78.9
LPA C22:1	491.2	152.9	78.9	cLPA C22:1	473.2	337.2	78.9
LPA C22:2	489.2	152.9	78.9	cLPA C22:2	471.2	335.2	78.9
LPA C22:4	485.2	152.9	78.9	cLPA C22:4	467.2	333.2	78.9
LPA C22:5	483.2	152.9	78.9	cLPA C22:5	465.2	331.2	78.9
LPA C22:6	481.2	152.9	78.9	cLPA C22:6	463.2	329.2	78.9

** Available Commercial standards which was used to define column retention and elution sequence.